CHAOS AND THE APPROACH TO EQUILIBRIUM IN THE DISCRETE SINE-GORDON EQUATION

by

C. G. Goedde, A. J. Lichtenberg, and M. A. Lieberman

Memorandum No. UCB/ERL M91/76

5 September 1991

CHAOS AND THE APPROACH TO EQUILIBRIUM IN THE DISCRETE SINE-GORDON EQUATION

by

C. G. Goedde, A. J. Lichtenberg, and M. A. Lieberman

Memorandum No. UCB/ERL M91/76

5 September 1991

ELECTRONICS RESEARCH LABORATORY

College of Engineering
University of California, Berkeley
94720

CHAOS AND THE APPROACH TO EQUILIBRIUM IN THE DISCRETE SINE-GORDON EQUATION

by

C. G. Goedde, A. J. Lichtenberg, and M. A. Lieberman

Memorandum No. UCB/ERL M91/76

5 September 1991

ELECTRONICS RESEARCH LABORATORY

College of Engineering
University of California, Berkeley
94720

Chaos and the Approach to Equilibrium in the Discrete Sine-Gordon Equation

C. G. Goedde[1]

Department of Physics

University of California, Berkeley, CA 94720

A. J. Lichtenberg and M. A. Lieberman

Department of Electrical Engineering and Computer Sciences

and the Electronics Research Laboratory

University of California, Berkeley, CA 94720

ABSTRACT

In this paper we study the long-time dynamics of a discretization of the sine-Gordon equation. We numerically investigate the system's approach to equipartition of energy when the initial energy is confined to one or a small set of Fourier modes. We find that there is a correspondence between the onset of chaos in the system, as evidenced by a sharp rise in the largest Lyapunov exponent, and a transition from a low energy regime in which energy does not spread appreciably among the modes to a high energy regime in which the system rapidly approaches equipartition. For low frequency initial conditions, the critical parameter for this transition is the scaled energy $E' = (L/N)^2 E$. Using a generalization of the traditional Chirikov resonance overlap calculation on a three mode subset of the full system, we predict the onset of chaos and the transition to equipartition.

---

[1]Current address: Department of Mathematics, The Ohio State University, Columbus, Ohio 43210.

Research sponsored by ONR Grant N00014-89-J-1097 and NSF Grant ECS-8910762.

1. Introduction

There is currently considerable interest in understanding the dynamical behavior of systems with many degrees of freedom. One question is whether the intrinsic stochasticity which appears in two degrees of freedom [1] tends to increasingly fill the phase space volume as the number of degrees of freedom increase. For example, it is well known that most of the phase space of two coupled nonlinear pendula may be chaotic, but it is not known whether this is generic when the number of coupled pendula is large. A related question is the extent of chaos in a nonintegrable discretization of an integrable nonlinear partial differential equation. Is there an identifiable transition between the behavior at coarse discretization (*i.e.* chaos in few degrees of freedom) and at fine discretization (integrability in the continuum limit). We are currently investigating this latter question in the context of a particular discretization of the sine-Gordon equation.

One of the earliest attempts to observe the behavior of a discretized nonlinear partial differential equation was made by Fermi, Pasta, and Ulam [2], who numerically examined the system

$$\ddot{x}_i = (x_{i+1} + x_{i-1} - 2x_i) + \beta[(x_{i+1} - x_i)^3 - (x_i - x_{i-1})^3]. \tag{1}$$

This corresponds to a set of equimass particles connected by nonlinear springs and is a spatial discretization of the equation

$$\frac{\partial^2 x}{\partial t^2} - \frac{\partial^2 x}{\partial z^2}\left[1 + 3\beta\left(\frac{\partial x}{\partial z}\right)^2\right] = 0. \tag{2}$$

The original result with 64 particles indicated that at low energy equipartition was not obtained among the oscillators, but rather a beat phenomenon existed with regular approximate recurrences of initial conditions. This result, contrary to the original expectation of

equipartition, stimulated a number of investigations [3–5]. It was found that transitions could occur with increasing energy from apparently regular to apparently irregular motion. These observations are consistent with the understanding of coupled systems of a few dimensions in which such transitions occur when resonances between degrees of freedom overlap in the action space [1]. In fact, Izrailev and Chirikov [5], using a normal mode expansion, developed an analytic overlap criterion which, in the few cases tested, appeared to roughly predict the numerical results.

More recently, Livi *et al* and Pettini and Landolfi have published a series of numerical studies of the FPU system [6–8]. They studied the statistical properties of the spatial Fourier expansion of the system (1) with periodic boundary conditions by introducing the spectral entropy,

$$h(t) = -\sum_{n=1}^{N/2} p_n(t) \ln p_n(t), \tag{3}$$

where $p_n(t) = E_n / \sum_i E_i$ is the fractional harmonic energy in the n^{th} Fourier mode, and N is the total number of modes. To eliminate the dependence on N of $h(t)$, they define the normalized quantity

$$\eta(t) = \frac{h_{\max} - h(t)}{h_{\max} - h(0)}. \tag{4}$$

The quantity η is bounded between zero and one, with zero corresponding to exact equipartition of energy.

The authors study the behavior of η given an initial condition in which a small number of low frequency (long wavelength) modes are equally excited. As they vary N and the total energy of excitation, E, they find that η is approximately a function of a single variable, the energy density $\epsilon = E/N$. The quantity η decays over some characteristic time scale, τ_R,

until it reaches a minimum value that is determined by the fluctuations of the energy of each mode around the equipartitioned state. Additionally, they calculate the maximum Lyapunov exponent, which is again a function of the energy density ϵ. They find that there is a critical value of ϵ at which the behavior of both λ and η change, and that above this energy density that the scaling of λ with ϵ can be explained using a random matrix approximation of the dynamics, which indicates that the phase space is strongly chaotic above the critical energy.

In this article we consider a similar dynamical system: a chain of linearly coupled pendula, which corresponds to a discretization of the sine-Gordon equation. Because of its usefulness in modelling physical systems, particularly in condensed matter physics [9], as well as its inherent mathematical interest [10], the sine-Gordon equation has been extensively studied, and is well known to be exactly solvable in terms of its fundamental soliton modes [11]. The discretization discussed here does not preserve the integrability of the system, and the motion of the discrete system is generically chaotic. It does present a natural physical model of the sine-Gordon equation, and a practical model system for studying the dynamics of high-dimensional Hamiltonian systems. The focus of this work is in understanding how the interaction of the Fourier modes of the system leads to chaotic motion and subsequent equipartion of energy.

In Section 2 we present the basic formulation of the discrete problem. In addition to the spatial discretization, a further discretization in time leads to a system of coupled standard maps. In addition to the intrinsic interest of this system of coupled maps, the mapping approximation allows one to greatly increase computational speed so that long times and large numbers of oscillators can be explored. If the mapping frequency is large compared to

all natural frequencies of the oscillator chain, then the dynamics is indistinguishable from the continuous time system over short times. For lower mapping frequencies, resonances between the mapping frequency and the normal mode frequencies can lead to parametric instabilities [12].

Section 3 presents numerical results on the system's approach to equilibrium and the behavior of the spectral entropy as the system's energy, length and number of oscillators are varied. We find for long wavelength initial conditions that there is a gradual transition from apparently regular motion at low energies to strongly chaotic motion at high energies, and that η is not a simple function of the energy density E/N as it is in the FPU problem, but that it is a function of EL^2/N^2. We also find that there is a rapid increase in the maximum Lyapunov exponent at the transition energy. In contrast, we find that short wavelength initial conditions exhibit a very sharp transition from apparently regular motion at low energy to strongly stochastic motion at high energy.

In Section 4, we present a calculation of the onset of resonance overlap in a three-mode truncation of the system. We expect that the existence of overlap will lead to strong chaotic motion in the system, resulting in the system's evolution toward equipartition of energy. The results of this calculation are then compared to the numerical results on equipartion of the full system.

2. Basic Formulation

The one-dimensional unperturbed sine-Gordon equation is

$$\phi_{tt} - \phi_{xx} + \sin\phi = 0, \tag{5}$$

where the time and space coordinates have been normalized to make the characteristic velocity and the pendulum frequency equal to unity, and all physical quantities are dimensionless. The space coordinate is discretized through the substitutions

$$\begin{aligned} \phi(x,t) &\longrightarrow \phi_j(t) \qquad j = 1, 2 \ldots N-1, \\ \phi_{xx}(x,t) &\longrightarrow \frac{[\phi_{j+1}(t) - \phi_j(t)] + [\phi_{j-1}(t) - \phi_j(t)]}{(\Delta x)^2}. \end{aligned} \tag{6}$$

We consider a spatial domain of length L, with fixed ends, such that $\phi_0 = \phi_N = 0$. The spacing between oscillators, Δx, is L/N. With the change of notation $\phi_j = q_j$, $\dot{\phi}_j = p_j$, the Hamiltonian for the discretized system can be written

$$H(\boldsymbol{q}, \boldsymbol{p}) = \sum_{i=1}^{N-1} \frac{1}{2} p_i^2 + \sum_{i=1}^{N-1} \Gamma^2 (1 - \cos q_i) + \sum_{i,j=1}^{N-1} \frac{1}{2} A_{ij} q_i q_j, \tag{7}$$

where the coupling matrix A_{ij} is given by

$$A_{ij} = \frac{(2\delta_{i,j} - \delta_{i,j+1} - \delta_{i,j-1})}{(\Delta x)^2}, \tag{8}$$

and where δ_{ij} is the Kronicker δ-function.

This Hamiltonian has the following physical interpretation: the first two terms correspond to $N-1$ pendula, and the last term represents harmonic coupling between nearest neighbors. The parameter Γ is a generalized linear frequency of the pendula. Taking $\Gamma = 1$ corresponds to the discretized sine-Gordon equation.

Since the linear part of this Hamiltonian (the first and third terms of (7)) is exactly solvable, it is useful to analyze the problem in terms of the normal modes of the harmonic springs. The eigenvectors of the linear system may be written as

$$e_{ir} = \frac{2}{\sqrt{N}} \sin \frac{\pi i r}{N}. \tag{9}$$

Note that the eigenvectors are orthonormal, $\sum_{i=1}^{N-1} e_{ir} e_{is} = \delta_{rs}$, as well as symmetric, $e_{ir} = e_{ri}$. We also define a new set of variables, $(\boldsymbol{u}, \boldsymbol{v})$, such that $(\boldsymbol{q}, \boldsymbol{p})$ can be represented as

$$q_i = \sum_{r=1}^{N-1} u_r e_{ir}, \qquad p_i = \sum_{r=1}^{N-1} v_r e_{ir}. \tag{10}$$

In terms of $(\boldsymbol{u}, \boldsymbol{v})$ the Hamiltonian becomes

$$H(\boldsymbol{u}, \boldsymbol{v}) = \sum_{r=1}^{N-1} \left[\frac{v_r^2}{2} + \omega_r^2 \frac{u_r^2}{2} \right] + \Gamma^2 \sum_{i=1}^{N-1} \left[1 - \cos \left(\sum_{r=1}^{N-1} u_r e_{ir} \right) \right] = H_0 + H_1. \tag{11}$$

This describes a system of $N-1$ harmonic oscillators, of frequencies $\omega_1 \ldots \omega_N$, coupled through the cosines. Since the number of oscillators is finite, the spectrum is discrete, with the (dimensionless) frequencies given by

$$\omega_r = \frac{2}{\Delta x} \sin \frac{\pi r}{2N} = \frac{2N}{L} \sin \frac{\pi r}{2N}, \tag{12}$$

with the maximum and minimum frequencies being

$$\omega_{\max} = \omega_{N-1} \simeq \frac{2N}{L}, \qquad \omega_{\min} = \omega_1 \simeq \frac{\pi}{L}. \tag{13}$$

When the problem is formulated in the $(\boldsymbol{u}, \boldsymbol{v})$ variables, it is natural to think of the linear system as the fundamental system, and the nonlinearity as a perturbation. However, we have not assumed that $H_1 \ll H_0$. In fact, there are three main regimes. For strong

springs, *i.e.* for $\omega_{\min} \gg \Gamma$, $H_1 \ll H_0$. For weak springs, $\omega_{\max} \ll \Gamma$, and $H_1 \gg H_0$. We will mostly be concerned with the intermediate range $\omega_{\min} \ll \Gamma < \omega_{\max}$, where $H_1 \sim H_0$.

The discretization has converted the infinite dimensional system described by a partial differential equation to a $2(N-1)$ dimensional system described by a set of coupled ordinary differential equations. A further discretization in time converts the system to a symplectic mapping. Physically, this is equivalent to pulsing gravity with period T. The discretization has the effect of adding an explicit time dependence to the Hamiltonian, so that energy is no longer conserved. The Hamiltonian (11) is modified by multiplying H_1 by an infinite series of delta functions to obtain

$$H_1 = \Gamma^2 \left(\sum_{i=1}^{N-1} \left[1 - \cos\left(\sum_{r=1}^{N-1} u_r e_{ir} \right) \right] \right) \left(\sum_{m=-\infty}^{\infty} \delta(t/T - m) \right). \tag{14}$$

The equations of motion are then

$$\dot{u}_s = v_s, \tag{15a}$$

$$\dot{v}_s = -\omega_s^2 u_s - \Gamma^2 \left(\sum_{m=-\infty}^{\infty} \delta(t/T - m) \right) \sum_{i=1}^{N-1} e_{is} \sin\left(\sum_{r=1}^{N-1} u_r e_{ir} \right). \tag{15b}$$

The delta functions allow (15) to be integrated by using the boundary conditions at $t = mT$:

$$\begin{aligned} u_s' - u_s &= 0, \\ v_s' - v_s &= -\Gamma^2 T \sum_{i=1}^{N-1} e_{is} \sin\left(\sum_{r=1}^{N-1} u_r e_{ir} \right). \end{aligned} \tag{16}$$

Here the primed [unprimed] variables denote quantities just after [before] a gravity pulse. The physical interpretation of (16) is that the positions are unchanged by the gravity pulse

and the momenta undergo an instantaneous change. The dynamics then evolve according to the area preserving map

$$u_s' = u_s \cos\omega_s T + \frac{1}{\omega_s}\left[v_s - \Gamma^2 T \sum_{i=1}^{N-1} e_{is} \sin\left(\sum_{r=1}^{N-1} u_r e_{ir}\right)\right] \sin\omega_s T, \tag{17a}$$

$$v_s' = -\omega_s u_s \sin\omega_s T + \left[v_s - \Gamma^2 T \sum_{i=1}^{N-1} e_{is} \sin\left(\sum_{r=1}^{N-1} u_r e_{ir}\right)\right] \cos\omega_s T. \tag{17b}$$

If the mapping period T is small, the mapping (17) well approximates the solution to the continuous system. For example, though the energy is no longer conserved, it will now oscillate around a constant value, which is indicative of an underlying constant of the motion. Iterating this mapping allows us to investigate the long time behavior of the discrete sine-Gordon system.

3. Numerical Results on the Approach to Equilibrium

In this section we present numerical results on how the approach to equilibrium changes as the important system parameters are varied. The typical initial conditions to be studied are excitations of a single linear mode described by (u_r, v_r). For convenience in specifying the initial energy, we choose the particular phase for which $u_r(0) = 0$ and $v_r(0) = \sqrt{2E}$. We will concentrate primarily on initial excitations of the fundamental linear mode $r = 1$. Note that the frequencies are ordered as $\omega_1 < \omega_2 \ldots < \omega_{N-1}$, so that a reference to mode r as a "low mode" or "low frequency mode" implies that $r \ll N$.

The calculations were performed on a CRAY-2 supercomputer. Parameters include a timestep for the mapping (17) of $T = 0.1$ and 10^6 iterations of the map for a total integration time of $t = 10^5$. As a check that the discreteness in time is not influencing the system's

behavior, certain initial conditions were integrated using a timestep of $T = 0.01$; these show the same behavior as the trials with $T = 0.1$.

Because of the nature of the nonlinearity, the system length L, which can be trivially scaled away in the FPU problem, is an important parameter in the discrete sine-Gordon problem. When performing numerical studies of the FPU problem, one is free to arbitrarily choose an oscillator spacing of unity, so that $N/L = 1$ (see, for example, [2,6–8]). For the discrete sine-Gordon system, the choice of L is intimately connected with the strength of the nonlinearity, and thus directly affects the behavior of the system. Because of this, N and L must be treated as independent parameters in the discrete sine-Gordon system.

The behavior of the energy distribution among the modes is made quantitative by means of the spectral entropy introduced by Livi *et al* [6–8]:

$$h(t) = -\sum_{n=1}^{N-1} p_n(t) \ln p_n(t). \tag{18}$$

Here $p_n(t)$ is the fractional harmonic energy in mode n,

$$p_n = \frac{E_n}{\sum_{i=1}^{N-1} E_i}, \qquad E_n = \frac{1}{2}(v_n^2 + \omega_n^2 u_n^2). \tag{19}$$

Because we are considering a chain with fixed ends, we have defined the sum in (18) over the $N-1$ modes, instead of the $N/2$ frequencies as in [6–8]. With this definition, the normalized quantity η is

$$\eta(t) = \frac{h_{\max} - h(t)}{h_{\max} - h(0)}, \tag{20}$$

with $h_{\max} = \ln(N-1)$.

Consider the set of parameters $N = 65$ and $L = 32$, with mode 1 initially excited. Figure 1 shows the behavior of $\eta(t)$ for three different initial energies. For low energies $\eta(t)$ oscillates

around a constant value. At intermediate energies, $\eta(t)$ is a slowly decreasing function of time. At high energy $\eta(t)$ falls rapidly to an equilibrium value. This progression is typical of low frequency initial excitations. At low energy, the energy remains confined among a few low frequency modes, while at high energy all modes are quickly excited, although the system never reaches exact equipartition, which would correspond to $\eta = 0$. For the high energy case, the equilibrium value of η is greater than zero because the energy is distributed about exact equipartition. It is possible to estimate what this equilibrium value of η should be by assuming that the dynamics is chaotic in the high energy regime.

This calculation, which assumes that the energies of the oscillators follow a Boltzmann distribution, is performed in the appendix, with the result

$$\eta_\infty = 0.423 \ln \frac{\Delta k}{N-1}. \tag{21}$$

Here Δk is the number of initially excited modes. For $N = 65$ and $\Delta k = 1$ (the parameters of (1)) this formula predicts $\eta_\infty = 0.102$, which is shown as the dashed line in Figure 1c. This prediction agrees very well with observed equilibrium value of η, and indicates that the equilibrium state of the system in this regime is chaotic.

In the low energy regime, the terminal value η_∞ can be estimated by

$$\eta_\infty = \frac{\ln\left((N-1)/\Delta m\right)}{\ln\left((N-1)/\Delta k\right)}. \tag{22}$$

This estimate assumes that the energy is shared equally among a small number of modes Δm. This is shown as the dashed line in Figure 1a for $\Delta m = 2$. The value of $\Delta m = 2$ was chosen because it was most representative of the the exponential fall off of the frequency spectrum seen in Figure 2b. The assumption of equally shared energy is too simplistic, however, since

the modes are continually exchanging energy. The oscillation of η between the values of 1 and 0.80 in Figure 1a indicates that the energy remains confined to a few modes, as seen in the snapshots of the power spectrum in Figure 2. For comparison, snapshots of the spectrum of the system in the chaotic regime are shown in Figure 3.

It is possible that the trajectory is not regular in the low energy regime, and that the curve in Figure 1a will eventually begin to drop. It is impossible to prove numerically that a given trajectory is not chaotic if the level of chaos is very low. However, numerical tests show that the curve in Figure 1a does not fall, and the energy remains confined in a few modes, even if iterated for a time of $t = 10^6$. Thus, we make the following hypotheses. For sufficiently small energy, the trajectory will be regular, and $\eta(t)$ will oscillate between 1 and a value which can be approximated by (22). For large energies, the trajectory is strongly stochastic, and η quickly falls to its equilibrium value given by (21). In the intermediate energy regime, $\eta(t)$ is a slowing decreasing function of the time, as seen in Figure 1b. For instance, if the integration time is increased by a factor of 10 to 10^6 for the case of Figure 1b, the equilibrium value of $\eta(t)$ shown in Figure 4 is obtained. This is in contrast to the very low energy case of Figure 1a, which is unchanged over longer integration times.

With these considerations in mind, we address the behavior of the value of η as a function of the energy at a long but fixed time. We find numerically that

$$\eta(E) = f\left(E\frac{L^2}{N^2}\right); \tag{23}$$

that is, η is a function, not of the energy E, or of the energy density E/N, as in the FPU problem, but of the scaled energy EL^2/N^2. We therefore introduce the scaled Hamiltonian

$$H' = \frac{L^2}{N^2}H = \sum_{r=1}^{N-1}\left[\frac{v_r^2}{2} + \omega_r^2\frac{u_r^2}{2}\right] + \frac{L^2\Gamma^2}{N^2}\sum_{i=1}^{N-1}\left[1 - \cos\left(\sum_{r=1}^{N-1}u_r e_{ir}\right)\right]. \tag{24}$$

Here v_r and ω_r have been rescaled by L/N, so that now $\omega_r = 2\sin(\pi r/2N)$, which results in a rescaling of the time by N/L. This rescaling of the time is important, since the value of $\eta(t)$ for intermediate energies is a function of the integration time. Note that all the times and energies presented in the figures in this section are these scaled times and energies.

Integrating the scaled Hamiltonian for a variety of parameters yields the universal curve shown in Figure 5. The abscissa of this figure is the value of the scaled Hamiltonian, which we call the scaled energy, and denote by E'. The result is truly remarkable in that the curve is seemingly independent of the "nonlinearity" parameter $L\Gamma/N$, which varies from 7.53 $(= 128/17)$ to 0.124 $(= 32/129)$ in Figure 5. The figure shows the transition (at $E' \sim 10$) between the low energy state where the initial condition is stable (or is unstable only on very long timescales) to the high energy regime where the system quickly relaxes to a nearly equipartitioned state. There is a spread in the curves at a fixed low scaled energy that can be understood from (22). At low energy, a number of modes are sharing energy in an essentially regular fashion. As N increases, the number of modes sharing energy (denoted by Δm in (22)) also increases, so η_∞ becomes smaller as N increases.

The corresponding maximum Lyapunov exponents are shown in Figure 6 for the same parameter values as the data in Figure 5. The exponent is calculated using the standard method [1]. The minimum Lyapunov exponent that can be measured numerically is a function of the time of integration. For the parameters used here, this minimum is $\lesssim 5 \times 10^{-5}$, which is seen in Figure 6 as the "long time" exponent at low energy. An examination of the time dependence of the exponent reveals that it is still falling according to $\lambda(t) \propto t$ in these cases, and the finite final value of λ is due to the finite integration time. As the energy of

the system is increased, the Lyapunov exponent rises quickly at $E' \sim 10$, which is the transition energy between the low and high energy regimes. This correspondence suggests that a transition from regular to chaotic dynamics is responsible for the decrease in the timescale necessary for equipartition.

The behavior of η shown in Figure 5 is typical of all low frequency initial conditions. For example, initial excitations of mode 2, or a combination of modes 1 and 3, all lie on the same universal curve.

The situation for initial excitations of high frequency modes is somewhat different. There is a general tendency for high modes to need more energy to reach equipartition. The behavior of $\eta(E')$ for an initial condition of mode 29 ($N = 65$ and $L = 32$) is shown in Figure 7. There are two important differences between this figure and Figure 5. The first is that the transition to evolution toward equipartition occurs at a much higher energy than for the low modes. The second is that the transition is much more abrupt for the high modes than for the low modes. There is a sudden jump from the regime where $\eta = 1$ to the regime where η quickly reaches its equilibrium value of η_∞. Both of these features are generic for high frequency initial excitations. This is in contrast to the range of transition energies for low modes, for which the system gradually moves from an apparently regular regime (Figure 1a) to an intermediate state where the decay toward equilibrium occurs very slowly, as typified in Figure 1b.

The sudden jump from $\eta = 1$ to $\eta = \eta_\infty$ in Figure 7 is evidence that below the transition energy the oscillations of mode 29 are indeed regular. This transition is further investigated in the high frequency case in Figure 8, in which the time needed for the system to reach

$\eta = 0.5$ is plotted versus energy. From the figure the delay time appears to approach infinity at the transition energy of $E' \sim 80$. This implies that the motion below this energy is indeed regular.

One interpretation of the difference in the results is that the local phase space in the neighborhood of the low frequency modes has a different geometric character from that of the high frequency modes. In the portion of phase space occupied by the low modes, we postulate that the phase space is mainly stochastic. However the local resonances generated by the nonlinear interaction may either overlap, causing strong stochasticity, or not overlap, in which case the weaker Arnold diffusion applies. In contrast, we postulate that the initial condition corresponding to the high frequency modes lie in a portion of the phase space that is primarily regular, until the energy becomes large. The probability of an initial condition lying in a stochastic layer, and the overlap that leads to strong stochasticity, occur nearly simultaneously. We investigate the mechanism for the low frequency mode transition in the next section.

4. Resonance Overlap

In the previous section we numerically examined the behavior of initial conditions where the energy was initially concentrated in a single linear mode. This mode quickly excited a small number nearby modes, and spread the energy among them, as shown in Figure 2, which shows the energy spectrum after approximately one tenth of the period of the initially excited mode. Once the driven modes have appreciable energy, there exists the possibility of resonances and resonance overlap between the modes. The interaction of these modes can

be understood in terms of an approximate Hamiltonian, which can be used to predict the onset of chaos.

The calculation in this section is based on the hypothesis that the interaction of the initially excited modes must be chaotic in order for the system to diffuse through the phase space. Given an initial condition where only a few modes have appreciable energy, if the motion of these modes is regular, then the energy should not spread to other modes. If their motion is chaotic, however, then the energy can be transported throughout the system. In order to estimate where this transition takes place we examine the interaction of the resonances that arise among the relevant interacting modes. The overlap calculation has two steps. The first is to determine which modes interact, since some modes are coupled strongly, some weakly. We derive the Hamiltonian that determines, for a given excitation, which modes are relevant to the dynamics. This Hamiltonian determines which modes interact, and how strongly.

The motion of a set of coupled oscillators is not necessarily chaotic, however. Once the form of the coupling of the modes is known, the second step of the calculation is to determine whether and how the modes resonate with each other. It is this resonance between the modes that may result in chaotic motion. Once the existence of chaotic motion is confirmed, it is necessary to determine the extent of the chaos. We use a simple extension of the two-dimensional Chirikov overlap criterion [1] to estimate the extent of the chaotic motion in a three-mode approximation of the full dynamics. We expect that the transition to rapid equipartition in the full system (as seen in Figure 5) will coincide with the transition to large-scale chaos in the three-mode dynamics.

Using the scaled Hamiltonian (24), and assuming that only one mode, with mode number a (a integer), is excited, the sum over the eigenmodes can be split into a large and a small piece:

$$\sum_{r=1}^{N-1} u_r e_{ir} = u_a e_{ia} + \sum_{\substack{r' \\ r' \neq a=1}}^{N-1} u_{r'} e_{ir'}. \tag{25}$$

This allows H_1 to be written as

$$H_1 = \alpha^2 \sum_{i=1}^{N-1} \left[1 - \cos\left(f_N u_a \sin \frac{\pi i a}{N} + \cdots \right) \right], \tag{26}$$

where we have set $\alpha = L\Gamma/N$ and $f_N = \sqrt{2/N}$ for notational convenience.

Keeping only the dominant mode, mode a, and expanding the cosine in (26) in terms of Bessel functions,

$$\begin{aligned} \cos(z \sin\theta) &= J_0(z) + 2 \sum_{k=1}^{\infty} J_{2k}(z) \cos 2kz, \\ \sin(z \sin\theta) &= 2 \sum_{k=1}^{\infty} J_{2k-1}(z) \sin(2k-1)\theta, \end{aligned} \tag{27}$$

yields

$$H' = \frac{v_a^2 + \omega_a^2 u_a^2}{2} + \alpha^2 \sum_{i=1}^{N-1} \left[1 - J_0(f_N u_a) - 2 \sum_{k=1}^{\infty} J_{2k}(f_N u_a) \cos \frac{2k\pi i a}{N} \right]. \tag{28}$$

Using the relations,

$$\sum_{i=1}^{N-1} \cos \frac{\pi i r}{N} = N \hat{\delta}_r - \frac{1 + \cos \pi r}{2}, \tag{29}$$

where $\hat{\delta}_r \equiv \delta_{r,mN}$, where m is an even integer, and

$$J_0(z) + \sum_{k=1}^{\infty} J_{2k}(z) = 1, \tag{30}$$

leads to

$$H' = \frac{v_a^2 + \omega_a^2 u_a^2}{2} + \alpha^2 N \left[1 - J_0(f_N u_a) - 2 \sum_{k=1}^{\infty} J_{2k}(f_N u_a) \hat{\delta}_{2ka} \right]. \tag{31}$$

This is the Hamiltonian for a single mode. The primary nonlinearity is contained in the term $J_0(f_N u_a)$; the last term is unimportant because the delta function will generally be satisfied only for large values of k, for which the Bessel functions are small. For example, if $a = 2$ and $N = 65$, then the only terms in this sum which are nonzero are when $k = 65m$, m integer.

Retaining two modes in the above procedure results in the interaction Hamiltonian for two modes (labelled by a and b):

$$\begin{aligned} H' = & \frac{v_a^2 + v_b^2}{2} + \frac{\omega_a^2 u_a^2 + \omega_b^2 u_b^2}{2} \\ & + \alpha^2 N \Bigg[1 - J_0(f_N u_a) J_0(f_N u_b) \\ & \qquad - 2 \sum_{k,k'=2}^{\infty E} J_k(f_N u_a) J_{k'}(f_N u_b) \left(\hat{\delta}_{ka-k'b} + \hat{\delta}_{ka+k'b} \right) \\ & \qquad + 2 \sum_{k,k'=1}^{\infty O} J_k(f_N u_a) J_{k'}(f_N u_b) \left(\hat{\delta}_{ka-k'b} - \hat{\delta}_{ka+k'b} \right) \Bigg] . \end{aligned} \tag{32}$$

This Hamiltonian describes the interaction of any two modes a and b. The strength of this interaction is determined by the order of the Bessel functions that couple the modes in question. The coupling terms are ordered according to the sum of the orders of the Bessel fuctions in each term. For example the term $J_3(f_N u_a) J_1(f_N u_b)$ is a fourth order term, and $J_6(f_N u_a) J_9(f_N u_b)$ is a $15th$ order term. The former corresponds to strong coupling of the modes, while in the latter case the modes would be weakly coupled. The terms are ordered in this way because $J_k(z) \sim z^k / k! 2^k$ for small z. Since the sums in the Hamiltonian (32) run to $k = \infty$, each mode is coupled to every other mode, but each mode is strongly coupled to only a few modes.

In order to apply this Hamiltonian to the full problem, consider an initial condition of the form used in section 3, where a single mode is excited, for example mode a. This mode

will then drive other modes, with the strength of the driving determined by the two-mode Hamiltonian (32). The most strongly driven mode will be the one whose interaction with the driving mode is given by the lowest order coupling term. This will be the term in the last sum of (32) when $k' = 1$, which leads to the selection rules

$$\begin{aligned} b &= 3a, && 0 < a < \frac{N-1}{3}, \\ b &= 2N - 3a, && \frac{N-1}{3} < a < \frac{2N}{3}, \\ b &= 3a - 2N, && \frac{2N}{3} < a < N. \end{aligned} \tag{33}$$

Given an initial excitation of mode a, mode b, as given by (33), will be the most strongly driven mode.

For example, if the initially excited mode is the fundamental mode $a = 1$, then the most strongly driven mode is $b = 3$, as seen in Figure 2b, in which only the odd modes are excited. In this case the Hamiltonian which describes the interaction of modes 1 and 3 is

$$\begin{aligned} H' = \frac{v_1^2 + v_3^2}{2} + \frac{\omega_1^2 u_1^2 + \omega_3^2 u_3^2}{2} \\ + \alpha^2 N \Big[1 - J_0(f_N u_1) J_0(f_N u_3) \\ - 2 \sum_{k=1}^{\infty} (-1)^k J_{3k}(f_N u_1) J_k(f_N u_3) \Big]. \end{aligned} \tag{34}$$

The factor $(-1)^k$ comes from the contribution of the sum over even k's in (32). In practice, only the $k = 1$ term of this sum is needed to accurately approximate the Hamiltonian.

Using the expansion techiniques described above, it is possible to calculate the interaction of an arbitrary number of modes. Unfortunately, the expanded coupling terms become very complicated when more than two terms are involved. However, the form of (32) indicates how the selection rules can be generalized when more than two modes are important.

For example, for 3 modes, the interaction terms will have the form

$$J_l(f_N u_a)J_m(f_N u_b)J_n(f_N u_c)\hat{\delta}_{la\pm mb\pm nc}. \tag{35}$$

For more than three modes, the general interaction term will be of the form (35), with one Bessel function for each mode, and with the appropriate delta function relating the mode numbers. For any given number of interacting modes, the most important coupling terms will of course be the lowest order terms.

The second step of the overlap calculation is to determine whether the interaction of the modes results in chaotic motion; this requires examining the resonances between the modes. In order to examine the resonances it is necessary to transform the system to the action-angle variables $(\boldsymbol{I}, \boldsymbol{\theta})$ of the unperturbed Hamiltonian (see, for example [1]). While it is possible to do this starting from an expanded form such as (32), it is more convenient to transform the unexpanded scaled Hamiltonian (24) to action-angle variables. Once the Hamiltonian is in action-angle form, the selection rules (33) can be used to pick out the important interactions.

In the regime of interest, where the generalized linear frequency, Γ, of the pendula is large compared to the smallest Fourier frequency, it necessary to explicitly include the quadratic part of the cosines in the linear part of the Hamiltonian H_0 before transforming to action-angle variables. Thus, we write the scaled Hamiltonian as

$$H' = \sum_{r=1}^{N-1}\left[\frac{v_r^2}{2} + (\omega_r^2 + \alpha^2)\frac{u_r^2}{2}\right] + \alpha^2 \sum_{i=1}^{N-1}\left[1 - \frac{u_i^2}{2} - \cos\left(\sum_{r=1}^{N-1} u_r e_{ir}\right)\right]. \tag{36}$$

With the notation $\Omega_r^2 = \omega_r^2 + \alpha^2$, $(\boldsymbol{I}, \boldsymbol{\theta})$ are given by

$$\begin{aligned} u_r &= \sqrt{2I_r/\Omega_r}\sin\theta_r, \\ v_r &= \sqrt{2\Omega_r I_r}\cos\theta_r. \end{aligned} \tag{37}$$

Using the transformation (37) in (36) yields

$$H' = \sum_{r=1}^{N-1} \Omega_r I_r + \alpha^2 \sum_{i=1}^{N-1} \left[1 - \frac{I_i \sin^2\theta_i}{\Omega_i} - \cos\left(\sum_{r=1}^{N-1} e_{ir}\sqrt{2I_r/\Omega_r}\sin\theta_r \right) \right]. \tag{38}$$

We first examine the resonances between two modes. As in the derivation of the two-mode Hamiltonian (32), we retain two terms in the sum over r in (38) and expand the cosines,

$$\begin{aligned} &\sum_{i=1}^{N-1} \cos\left(e_{ia}\sqrt{2I_a/\Omega_a}\sin\theta_a + e_{ib}\sqrt{2I_b/\Omega_b}\sin\theta_b \right) \\ &\quad = \sum_{i=1}^{N-1} \Bigg[\left(J_0(X_{ia}) + 2\sum_{k=1}^{\infty} J_{2k}(X_{ia})\cos 2k\theta_a \right) \\ &\qquad \times \left(J_0(X_{ib}) + 2\sum_{k'=1}^{\infty} J_{2k'}(X_{ib})\cos 2k'\theta_b \right) \\ &\qquad - 4\sum_{k,k'=0}^{\infty} J_{2k+1}(X_{ia})\sin(2k+1)\theta_a \\ &\qquad\qquad \times J_{2k'+1}(X_{ib})\sin(2k'+1)\theta_b \Bigg], \end{aligned} \tag{39}$$

where $X_{ir} \equiv e_{ir}\sqrt{2I_r/\Omega_r}$. Using this expansion in (38) yields the Hamiltonian for the two-

mode system,

$$
\begin{aligned}
H' = \Omega_a I_a + \Omega_b I_b - \frac{\alpha^2 I_a \sin^2\theta_a}{\Omega_a} - \frac{\alpha^2 I_b \sin^2\theta_b}{\Omega_b} \\
+ \alpha^2 \sum_{i=1}^{N-1} \Bigg[1 - \left(J_0(X_{ia}) + 2\sum_{k=1}^{\infty} J_{2k}(X_{ia}) \cos 2k\theta_a \right) \\
\times \left(J_0(X_{ib}) + 2\sum_{k'=1}^{\infty} J_{2k'}(X_{ib}) \cos 2k'\theta_b \right) \\
+ 4 \sum_{k,k'=0}^{\infty} J_{2k+1}(X_{ia}) \sin(2k+1)\theta_a \\
\times J_{2k'+1}(X_{ib}) \sin(2k'+1)\theta_b \Bigg].
\end{aligned}
\tag{40}
$$

This form of the Hamiltonian does not contain explicit information about which modes will interact; instead it describes the interaction of resonances between the modes. It is important to note that (40) is completely equivlent to (32). The expansion used to derive (32) was designed to exhibit the *strength* of the coupling between different modes. In contrast, the expansion in action-angle variables used to derive (40) was chosen to make the *resonances* between the modes explicit. The information about the strength of the interaction is contained in (40); it is implicit in the sum over the eigenvectors that are contained in X_{ia}. It would be possible to further expand this Hamiltonian to obtain the delta-function relationships embodied in (35). In practice, this is not necessary; since we already know which modes will interact (from (35)), we can choose the mode numbers a and b as appropriate. In particular, for low frequency modes, the proper choice is $b = 3a$.

The general form of the resonance condition is $m\dot{\theta}_a = n\dot{\theta}_b$; as can be seen from the form of (40), a resonance is possible only if both m and n are even or odd. In practice, the 1:1 resonance is the only first order resonance that exists for the low-mode interactions. This is

because $\Omega_r = \sqrt{\omega_r^2 + \alpha^2}$ is dominated by α^2, which is independent of mode number, so that the frequencies of the low frequency modes are nearly equal.

The position and size of the resonaces can be calculated using the method of averaging [1]. To examine the system near the 1:1 resonance, first transform to fast and slow variables:

$$\begin{aligned} \theta_s &= \theta_b - \theta_a, & I_a &= I_f - I_s, \\ \theta_f &= \theta_a, & I_b &= I_s. \end{aligned} \tag{41}$$

Averaging over θ_f leads to

$$\begin{aligned} H' = &\left(\Omega_a - \frac{\alpha^2}{2\Omega_a}\right) I_a + \left(\Omega_b - \frac{\alpha^2}{2\Omega_b}\right) I_b \\ &+ \alpha^2 \sum_{i=1}^{N-1} \left[1 - 2\sum_{k=1}^{\infty} J_k(X_{ia}) J_k(X_{ib}) \cos\theta_s\right]. \end{aligned} \tag{42}$$

For simplicity we have expressed this Hamiltonian in the original actions, I_a and I_b, instead of the slow and fast actions. The phase space of the Hamiltonian (42) is illustrated for two values of the fast action in Figure 9. The phase space contains a large island at $\theta_s = \pi$ which persists from low energies ($E' \simeq 2$ in Figure 9a) to high energies ($E' \simeq 150$) in Figure 9c). At intermediate energies there are several islands, as seen in Figure 9b for $E' \simeq 20$. The positions of all these island may be easily calculated from $\partial H'/\partial I_s = 0$ and $\partial H'/\partial \theta_s = 0$. At very high energies the 1:1 resonance disappears; this is the limit where the pendula are rotating rapidly and their angles are undergoing large excursions. In this case, the assumption that the pendulum frequency is dominated by its linear part is no longer valid, and the low-frequency modes no longer have nearly the same frequency.

The averaged system can be compared to a surface of section mapping of the exact two degree of freedom system (40). A section taken at $\theta_a = 0$ is shown in Figure 10 for

approximately the same energies as seen in Figure 9a–b. (At the very high energies of Figure 9c, the entire phase space is chaotic.) At low and intermediate energies, the agreement between the averaged phase space, shown in Figure 9, and this surface of section is quite good. The surface of section is of interest because it illustrates the mechanism for chaos in the two-mode system. The chaos does not grow out of the separatrix motion, as in the standard map; instead there is a higher order interaction near the elliptic fixed point at $\theta_s = \pi$ which causes an orbit near the elliptic fixed point to break up. This behavior is typical of intrinsically degenerate systems [1]. Numerical results indicate that the chaos results from a 1:1 resonance between the period of the orbits around the fixed point and the period at which the trajectory intersects the surface of section.

Rather than performing the analysis of this higher order resonance, we introduce a third mode and examine the multiple first order resonances which are present. Modes a, $3a$ and $5a$ will be the primary interacting modes; this is easily deduced from the general interaction term (35). The strongest resonances between these modes are the two 1:1 resonances between modes a and $3a$ and between modes a and $5a$.

The procedure for expanding the Hamiltonian in the three mode case is the same as in the two mode case: three terms are retained in the cosine in the last term of (38), which is then expanded using (27). Expressing the resulting Hamiltonian in the slow and fast variables near the two 1:1 resonances,

$$\begin{aligned} \theta_s &= \theta_{3a} - \theta_a, & I_a &= I_f - I_s - I_\sigma, \\ \theta_\sigma &= \theta_{5a} - \theta_a, & I_{3a} &= I_s, \\ \theta_f &= \theta_a, & I_{5a} &= I_\sigma, \end{aligned} \tag{43}$$

and averaging over θ_f, we obtain the averaged Hamiltonian for the three mode system,

$$\begin{aligned} H' = &\left(\Omega_a - \frac{\alpha^2}{2\Omega_a}\right) I_a + \left(\Omega_{3a} - \frac{\alpha^2}{2\Omega_{3a}}\right) I_{3a} + \left(\Omega_{5a} - \frac{\alpha^2}{2\Omega_{5a}}\right) I_{5a} \\ &+ \alpha^2 \sum_{i=1}^{N-1} \Bigg[1 - J_0(X_{ia}) J_0(X_{i,3a}) J_0(X_{i,5a}) \\ &\qquad - 2J_0(X_{i,5a}) \sum_{k=1}^{\infty} J_k(X_{ia}) J_k(X_{i,3a}) \cos k\theta_s \\ &\qquad - 2J_0(X_{i,3a}) \sum_{k=1}^{\infty} J_k(X_{ia}) J_k(X_{i,5a}) \cos k\theta_\sigma \Bigg]. \end{aligned} \tag{44}$$

Since θ_f does not appear in this Hamiltonian, $I_f = I_a + I_{3a} + I_{5a}$ is a constant of the motion.

The topology of mode overlap when three modes are present is quite different than the usual two-dimensional topology, and is shown in Figure 11. In this case the resonant surfaces are two dimensional, and generically intersect. Figure 11 shows this intersection inside the energy surface, which is denoted by E. For the specific problem at hand, the energy surface can be adequately approximated by the surface I_f = constant. This is possible since the frequencies of the modes are approximately equal, so that

$$H' \simeq \Omega_a I_a + \Omega_{3a} I_{3a} + \Omega_{5a} I_{5a} \sim \Omega_a I_f. \tag{45}$$

Since the resonances intersect, there is no obvious overlap criterion in this space, as in two dimensions. As before, however, each resonance will be surrounded by an island, which will give the resonant curves a finite width in the energy shell. These areas will overlap; inside this overlapped region the motion will be strongly chaotic. Since the energy shell is bounded, this overlapped area will occupy some fraction of the available action space. We propose to use the fraction of the action space in which this strong overlap occurs as a measure of the global stochasticity of the system.

The position and size of the islands can again be calculated by averaging. If the Hamiltonian (44) is averaged over one angle, for example θ_σ, then the corresponding action, I_σ, will be a constant of the motion. Then the position of the resonance and the size of the surrounding island (which is in the direction of the remaining action, I_s in this case) can be calculated from the resulting one dimensional Hamiltonian. The position and size of the second resonance can be calculated in the same manner.

Figure 12 shows the (I_s, I_σ) plane for a value of I_f corresponding to $E' = 20$. Since the original actions, I_a, I_{3a}, and I_{5a} are all non-negative, the space is bounded as the triangle in Figure 12 with $I_s + I_\sigma \leq I_f$. Within this space are the two resonance curves that correspond to the 1:1 resonances between modes a and $3a$ and modes a and $5a$, shown as the dashed lines. The width of each island extends from $I = 0$ to the solid line in the figure. As can be seen, the resonant curves cross, and the islands overlap, with the region of overlap in the lower lefthand part of the figure. It is then a simple matter to calculate the fraction of the action space that is overlapped. In Figure 12, the fraction of the available space in which strong overlap occurs is $\sim 30\%$.

The overlapped fraction as a function of the scaled energy E' is shown in Figure 13 for the same set of parameters as Figure 5. There is a rough correspondence between the energy for the onset of significant overlap and the onset of rapid equipartition in Figure 5. This suggests that the main hypothesis of this chapter is true—that the onset of rapid equipartition is correlated to the onset of global chaos in the relevant modes. When the overlapped region is small, the dominant mechanism for diffusion is slow Arnold diffusion along the resonances. This corresponds to the slow diffusion regime where $\eta(t)$ is a slowly

falling function of time. When the overlapped region is significant, however, the diffusion is rapid, and the system rapidly approaches equilibrium.

There are some other notable features of Figure 13. In the cases where $N > L$, the fraction of overlap begins to fall at high energy. This is because the system is leaving the regime where the pendulum frequency dominates the springs, so the island size falls, as was seen in Figure 9c. This occurs at lower energies when $N > L$ because of the way the Hamiltonian has been scaled; smaller L/N corresponds to stronger springs. At high enough energy, the overlap fraction eventually falls for all values of N and L. A second feature is that the overlap fraction increases more quickly at low E' for large N. This is because the frequency difference between the modes is inversely proportional to N, so it is easier to resonate at lower energy as N get larger.

There is one important difference between the information contained in the overlap scaling presented in Figure 13 and the scaling of η presented in Figure 5. The overlapped fraction describes the relative size of the chaotic region, but does not give direct information about the rate of diffusion through that region. While it is true for a given L and N that a larger region of overlap corresponds to stronger chaos and faster diffusion, there is no way to compare the relative diffusion rates for different values of N based on the size of the overlapped region.

On the other hand, Figure 5 contains explicit time information. Each different set of parameters is integrated for the same length of time (relative to the scaled energy E'), and at the end of the integration η is calculated. This scaling of the integration time with N and L is an important aspect of Figure 5. We should emphasis that this is a completely numerical

result; there is no theoretical reason why this time scaling should yield the universal curve seen in Figure 5.

For comparison, the time scaling can be taken out of Figure 5, and the results are shown in Figure 14. This figure was produced by integrating the unscaled Hamiltonian (11) for an equal amount of time for each set of parameters. From this figure it can be seen that without the time rescaling, the large values of N move toward equipartition more rapidly than low values of N. This is in agreement with the scaling of the size of the overlapped region. The large N values have large overlap at lower energy, and can therefore move toward equipartition at a lower energy. Thus it is clear that some detailed information about the diffusion rate is necessary to completely understand the scaling behind Figure 5.

5. Conclusions and Discussion

We have been concerned with the dynamics of a discretization of the sine-Gordon equation in space and time. The spatial discretization transforms the equation into a set of coupled pendula, and the further discretization in time gives a set of coupled standard maps. We investigated the conditions under which the energy in this system will be distributed in a statistical manner by studying the evolution of the system in which the energy was confined initially to one or a few Fourier modes.

In section 3 we numerically investigated the stability of initial conditions in which a single Fourier mode of the system was excited. For low frequency initial conditions, we found that the discrete sine-Gordon system undergoes a transition, with the critical parameter being the scaled energy $E' = (L/N)^2 E$, from a regime where such initial conditions are

stable, and the energy is spread among only a few modes, to a regime where the energy is spread throughout the entire system with an apparently statistical distribution. As this transition takes place there is a concurrent transition in the value of the maximum Lyapunov exponent from a near-zero value to a non-zero one. This correspondence indicates that the onset of rapid equipartition is related to the onset of large scale chaotic motion in the system.

For low frequency initial conditions, three important regimes have been studied. At high energy there is a rapid approach to equilibrium and the maximum Lyapunov exponent is large. At low energy, the system stays near its initial configuration. It is unknown whether the dynamics in this regime are regular or chaotic, but numerical evidence indicates that it is regular. In the low energy regime, the modes are still coupled, and there is an exchange of energy among a few strongly coupled modes. At intermediate energies, the system slowly relaxes to the equipartitioned state. In this regime the dynamics are chaotic, but more weakly chaotic than the high energy dynamics, and the diffusion is correspondingly slower.

For high frequency modes, the transition between strongly chaotic and regular motion is very sharp as the energy is varied. There is no intermediate regime where the diffusion is slow. Instead, the system is characterized near the transition by a delay time for the approach to equilibrium. As the transition is approached from above, numerical evidence indicates that this delay time apparently approaches infinity. This implies that the motion below the transition energy is regular.

Unlike systems with two degrees of freedom, whose phase space can be viewed in a two dimensional surface of section, direct visualization of the phase space for large-dimensional systems is difficult. However, it is possible to think schematically about the topology of the

space. In particular, the phase space contains many resonance surfaces, which generically intersect in more than two degrees of freedom. Chaos in the system is generated along the resonance curves, so these curves are really resonant bands with finite thickness. This thickness depends on the nonlinearity parameter, which is related to the energy in the system. The rate of diffusion along resonances is generally much slower than the rate across resonances. Thus, when the bands are narrow, and therefore not significantly overlapped, the diffusion is very slow. When the bands are large, their area of overlap is significant, and the diffusion through the phase space is much faster. The fast diffusion due to resonance overlap appears to be responsible for the rapid approach to equilibrium at large energies.

This hypothesis was tested using a resonance overlap calculation developed in section 4. The method is a generalization of the usual two-degree-of-freedom overlap calculation, which provides a way of estimating when isolating KAM tori are destroyed, so that global diffusion is possible. In systems with more than two degrees of freedom, global diffusion around invariant tori is possible because the resonance surfaces generically intersect. The generalized overlap criterion proposed here is a method to estimate when fast diffusion is significant in a system with three degrees of freedom. For the type initial conditions where all the energy is confined to a single linear mode, the nonlinearity rapidly spreads the energy to a few strongly interacting modes. Choosing the three most strongly interacting modes results in a three-mode approximation of the relevant dynamics of the system on short time scales. In the regime where the pendulum motion dominates, when $L \gg 1$, the low-frequency modes have approximately the same frequency, so a set of 1:1 resonances exists among the interacting modes. The position and width of each resonant band are individually calculated

using the method of averaging. The relative area of the overlap of these resonant bands is then used as a predictor of fast diffusion in the system.

The general agreement between the overlap calculation and the transition to equipartition is fairly good. The fraction of the action space occupied by strong overlap becomes significant at approximately the same energy that the rapid approach to equilibrium sets in.

Appendix

In this appendix we estimate the long time value of $\eta(t)$ for a fully stochastic Hamiltonian system. Consider a system of weakly coupled harmonic oscillators described by the Hamiltonian

$$H = \sum_{i=1}^{N-1} \omega_i I_i + H_1(\boldsymbol{I}, \boldsymbol{\theta}). \tag{A.46}$$

If the number of oscillators is large and the dynamics is ergodic, the energy distribution of the oscillators is described by the Boltzmann distribution

$$f_i \propto e^{-\beta \omega_i I_i}. \tag{A.47}$$

Here $f_i dI_i$ is the fraction of the oscillators lying between energy $E_i = \omega_i I_i$ and energy $E_i + dE_i = \omega_i(I_i + dI_i)$. The average energy is then

$$\langle E \rangle = \frac{\int \omega_i I_i e^{-\beta \omega_i I_i} dI_i d\theta_i}{\int e^{-\beta \omega_i I_i} dI_i d\theta_i} = \frac{1}{\beta}, \tag{A.48}$$

and the total energy of the system is just $E_T = N\langle E \rangle$. The distribution of energies about $\langle E \rangle$ described by (A.47) determines the equilibrium value of η.

Defining the equilibrium value of $h(t)$ to be the integral over the orbit, then, because the orbit is assumed to be ergodic, h_∞ can be written in terms of the distribution function

$$h_\infty = \sum_{i=1}^{N-1} \frac{\int (\omega_i I_i / E_T) \ln (\omega_i I_i / E_T) \, e^{-\beta \omega_i I_i} dI_i}{\int e^{-\beta \omega_i I_i} dI_i}. \tag{A.49}$$

The integrals are easily performed, yielding

$$h_\infty = \ln N - (1 - \boldsymbol{C}), \tag{A.50}$$

where $\boldsymbol{C} = 0.577\ldots$ is Euler's constant. Using this value in equation (18) gives an estimate of the equilibrium value of η:

$$\eta_\infty = 0.423 \ln \frac{\Delta k}{N-1}, \tag{A.51}$$

since $h(0) = \ln \Delta k$ when Δk modes are initially equally excited.

References

1. A. J. Lichtenberg and M. A. Lieberman, *Regular and Stochastic Motion* Springer-Verlag, N. Y. 1983.
2. E. Fermi, J. R. Pasta and S. Ulam, "Studies of Nonlinear Problems" in *Collected Works of Enrico Fermi* University of Chicago Press, Chicago 1965.
3. R. L. Bivins, N. Metropolis and J. R. Pasta, J. Comput. Phys. **12** 65 (1973).
4. J. Ford and J. Waters, J. Math. Phys. **4** 1293 (1963).
5. F. M. Izrailev and B. V. Chirikov, Sov. Phys. Dokl. **11** 30 (1966).
6. R. Livi, M. Pettini, S. Ruffo, M. Sparpaglione and A. Vulpiani, Phys. Rev. A **28** 3544 (1983).
7. R. Livi, M. Pettini, S. Ruffo, M. Sparpaglione and A. Vulpiani, Phys. Rev. A **31** 1039 (1985).
8. M. Pettini and M. Landolfi, Phys. Rev. A **41** 768 (1990).
9. A. R. Bishop, J. A. Krumhansl and S. E. Trullinger, Physica **1D** 1 (1980).
10. R. Flesch, M. G. Forest and A. Sinha, Physica **48D** 169 (1991).
11. M. J. Ablowitz, D. J. Kaup, A. C. Newell and H. Segur, Phys. Lett., **30** 1262 (1973).
12. C. G. Goedde, A. J. Lichtenberg and M. A. Lieberman, Physica **41D** 341 (1990).

Figure Captions

Figure 1. The time dependence of $\eta(t)$ for three different energies with $N = 65$ and $L = 32$. a) $E' = 2$. b) $E' = 8$. c) $E' = 32$.

Figure 2. Snapshots of the spectrum for $N = 65$, $L = 32$ and $E' = 2$, with an initial excitation of mode 1. Note how the energy oscillates among a small number of low frequency modes. a) $t = 1$. b) $t = 10^5$.

Figure 3. Snapshots of the spectrum for $N = 65$, $L = 32$ and $E' = 24$, again with an initial excitation of mode 1. In this case the energy spread throughout the system. a) $t = 1$. b) $t = 10^5$.

Figure 4. $\eta(t)$ in the chaotic region for $N = 65$, $L = 32$ and $E' = 8$ integrated for time $t = 10^6$.

Figure 5. The universal curve for $\eta(E')$.

Figure 6. The energy dependence of $\lambda(E')$ for the same parameter range as Figure 5.

Figure 7. The energy dependence of $\eta(E')$ when mode 29 is initially excited ($N = 65$). Note the sharp transition from $\eta = 1$ to $\eta = \eta_\infty$ at $E' \simeq 80$.

Figure 8. The time necessary for $\eta(t)$ to fall to 0.5. Note that the curve appears to asymptote at $E' \simeq 80$.

Figure 9. The phase space of the two-mode system averaged near the 1:1 resonance. $N = 65$, $L = 32$. a) $I_f = 5$, $E' \sim 2$. b) $I_f = 50$, $E' \sim 20$. c) $I_f = 500$, $E' \sim 150$.

Figure 10. A two-dimensional surface of section of the two-mode system taken at $\theta_f = 0$. $N = 65$, $L = 32$. a) $E' = 2$. b) $E' = 14$.

Figure 11. A schematic representation of the action space of a generic three-degree-of-freedom Hamiltonian system.

Figure 12. The resonance curves for the averaged three-mode system and their associated island widths. The position of the resonances is shown by dashed lines, and the island widths by solid lines. The region of strong overlap is the region in the lower left hand corner bounded by solid lines.

Figure 13. The fraction of the action space which is strongly overlapped as a function of E' for the same set of parameters as Figure 5.

Figure 14. The behavior of $\eta(E')$ when the time of integration is not scaled with N/L.

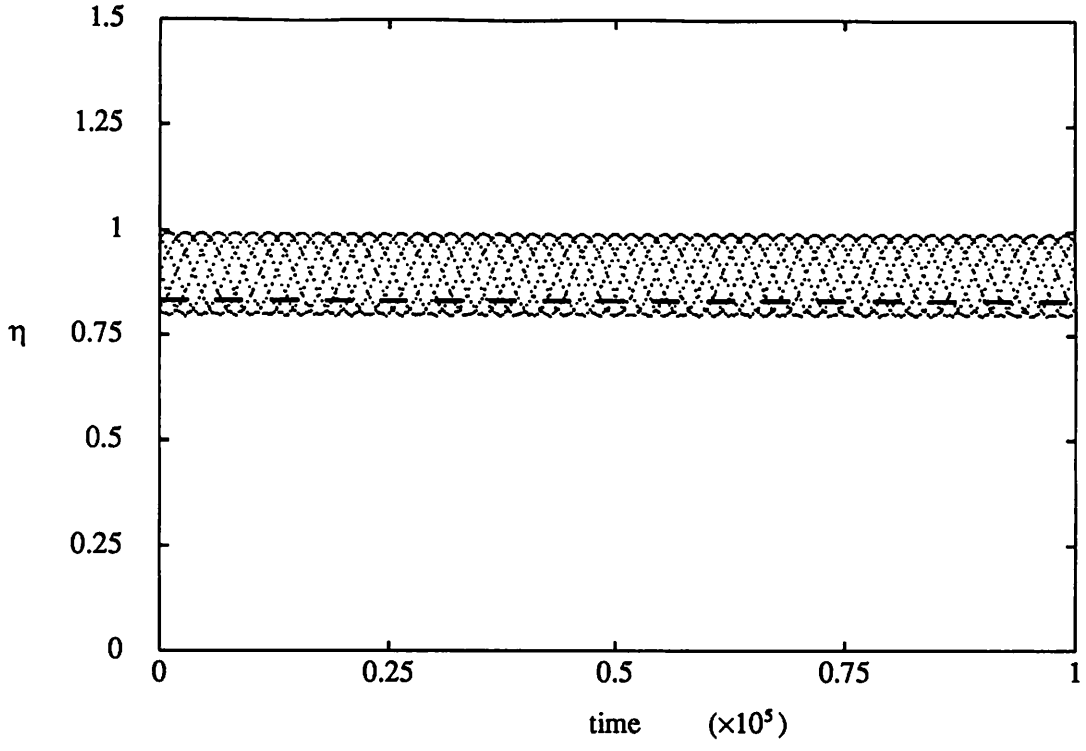

Figure 1a

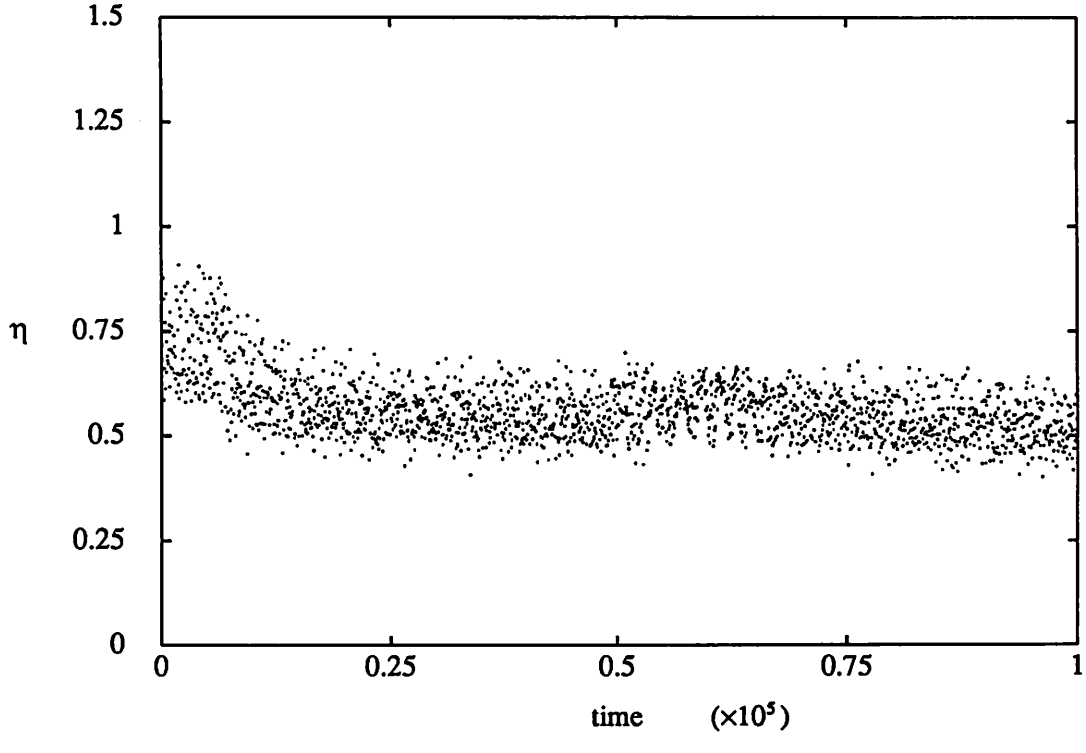

Figure 1b

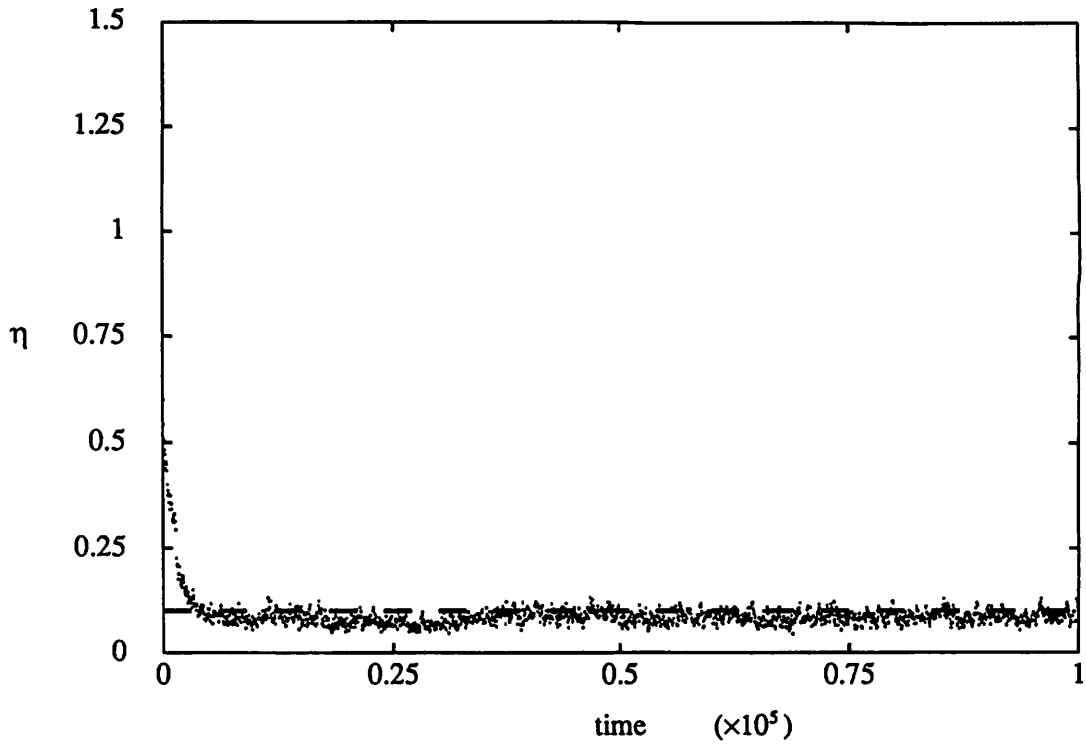

Figure 1c

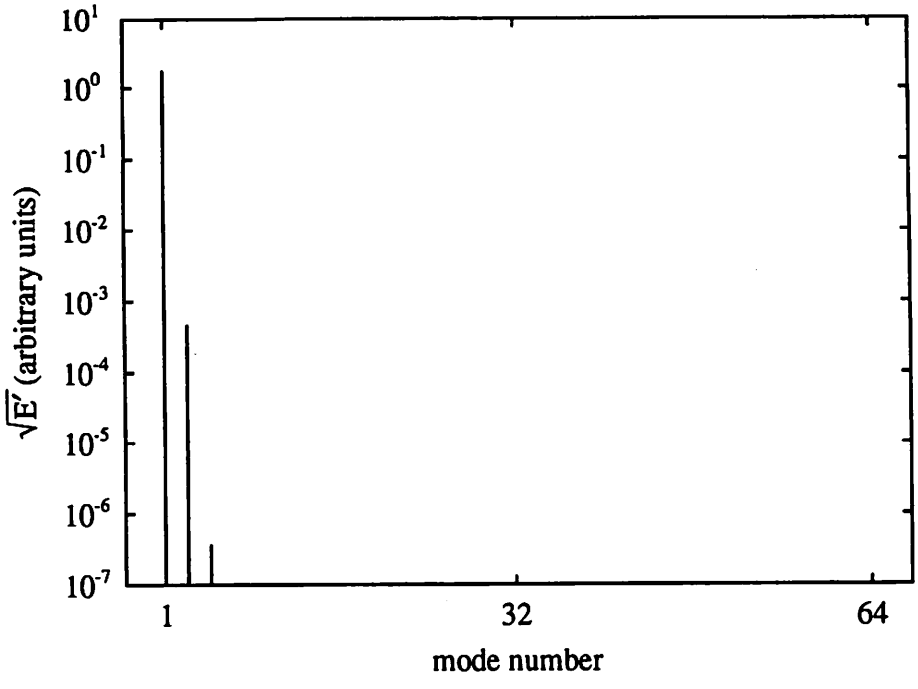

Figure 2a

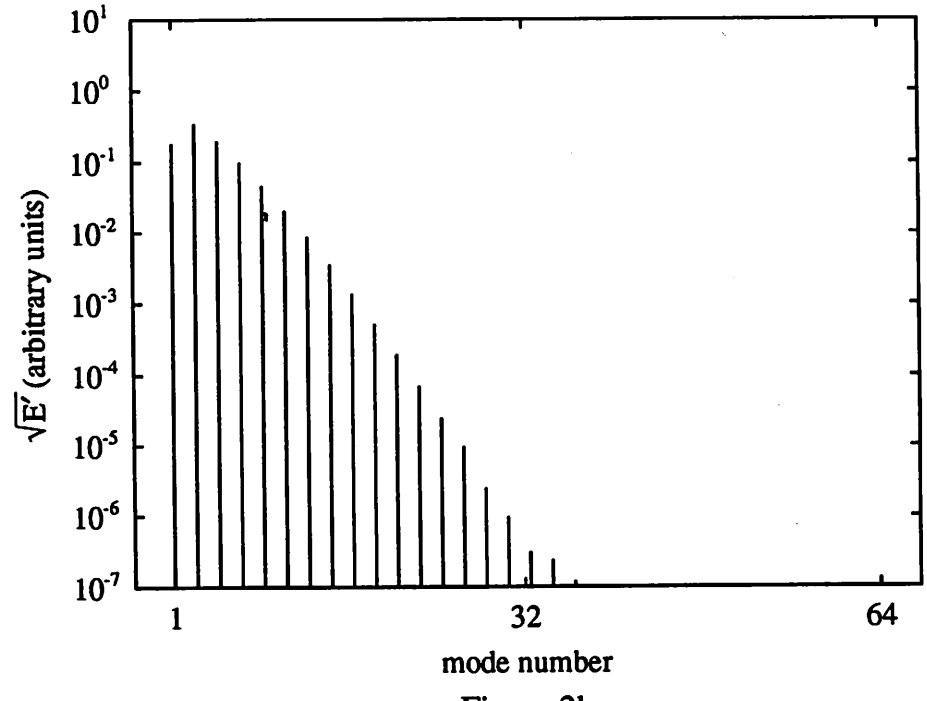

Figure 2b

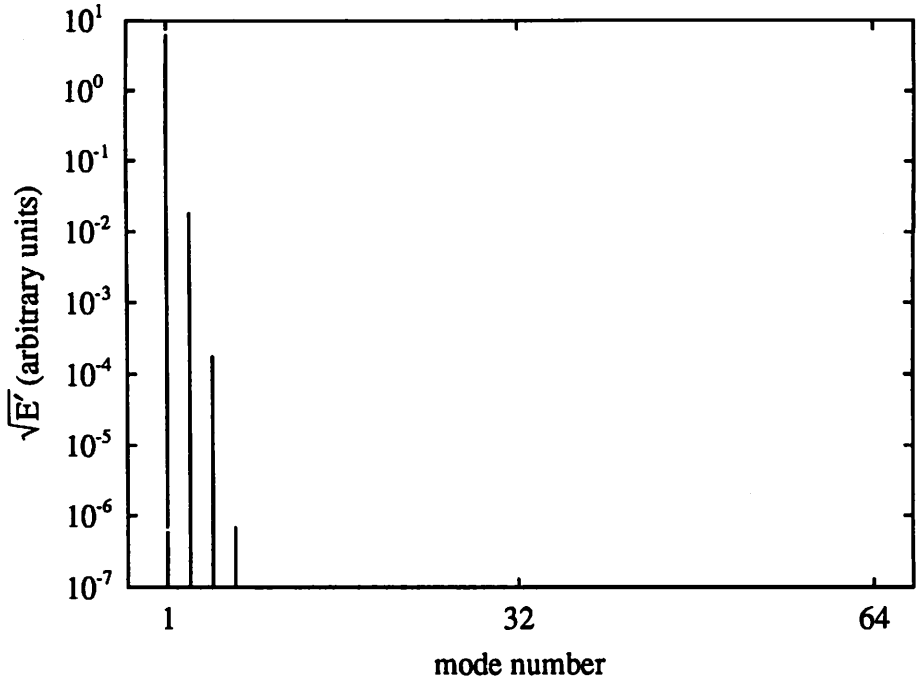

Figure 3a

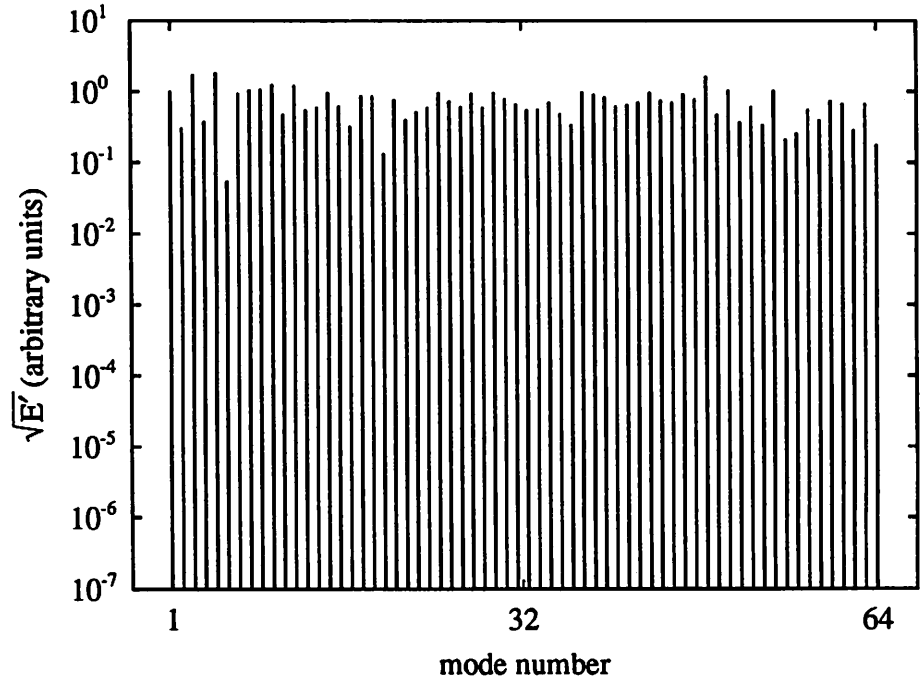

Figure 3b

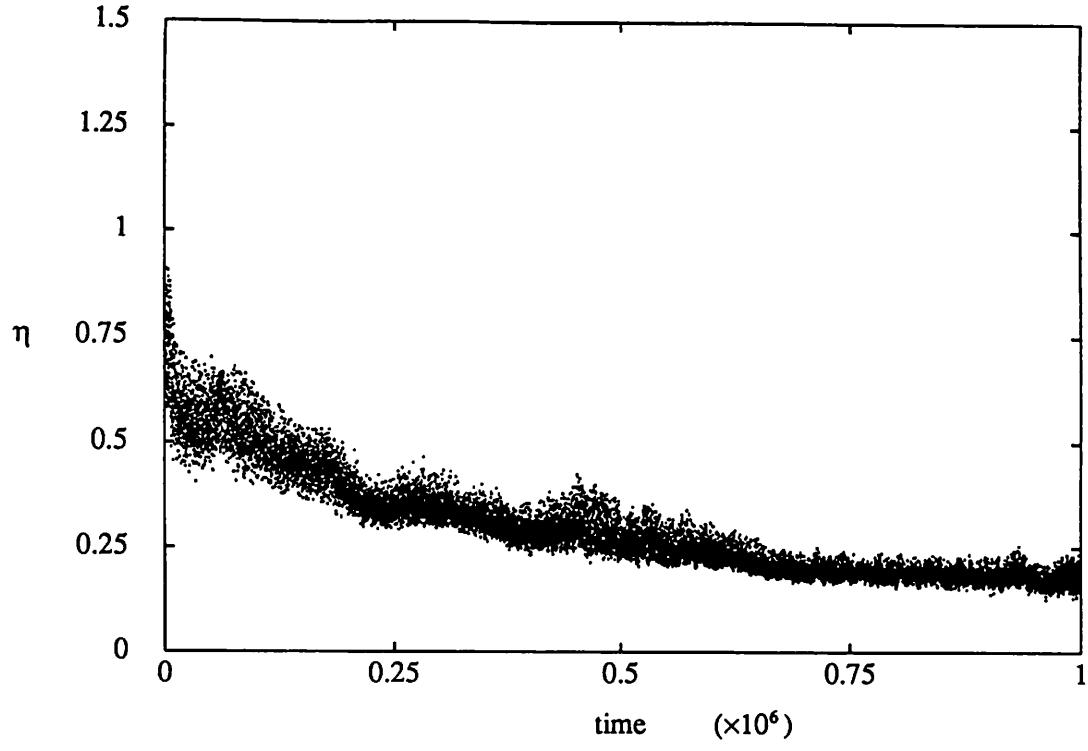

Figure 4

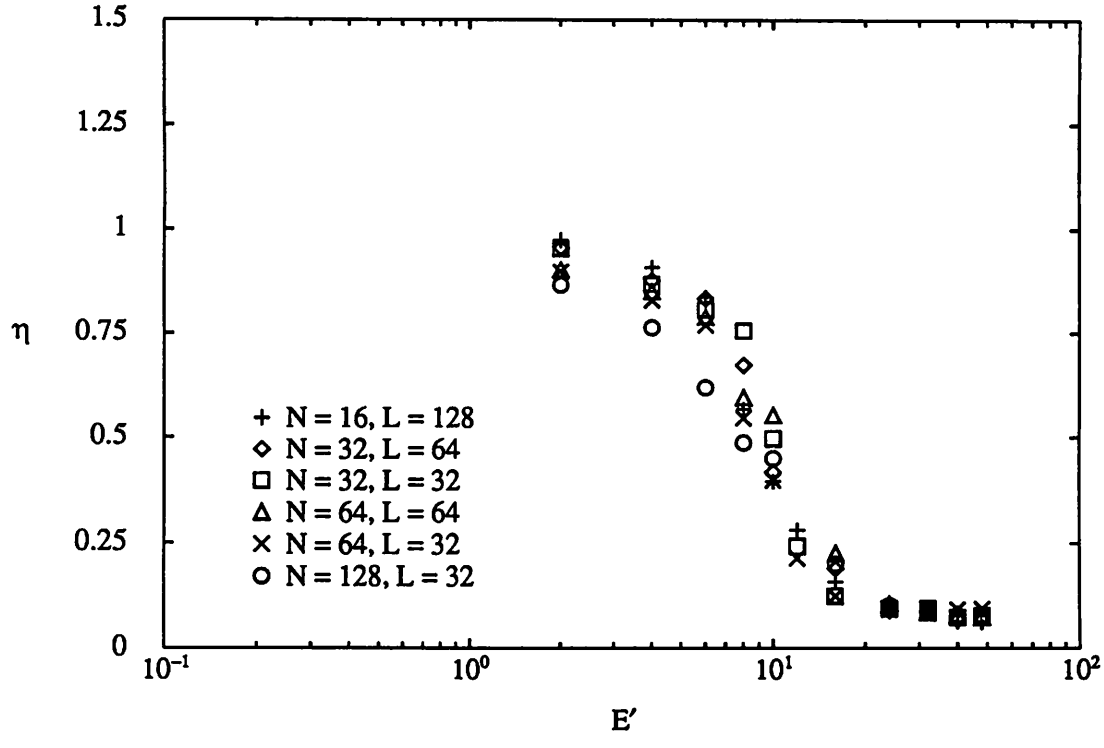
1.5
1.25
1
0.75
0.5
0.25
0
η
10^{-1}
10^{0}
10^{1}
10^{2}
E′
+ N = 16, L = 128
◇ N = 32, L = 64
□ N = 32, L = 32
△ N = 64, L = 64
× N = 64, L = 32
○ N = 128, L = 32

Figure 5

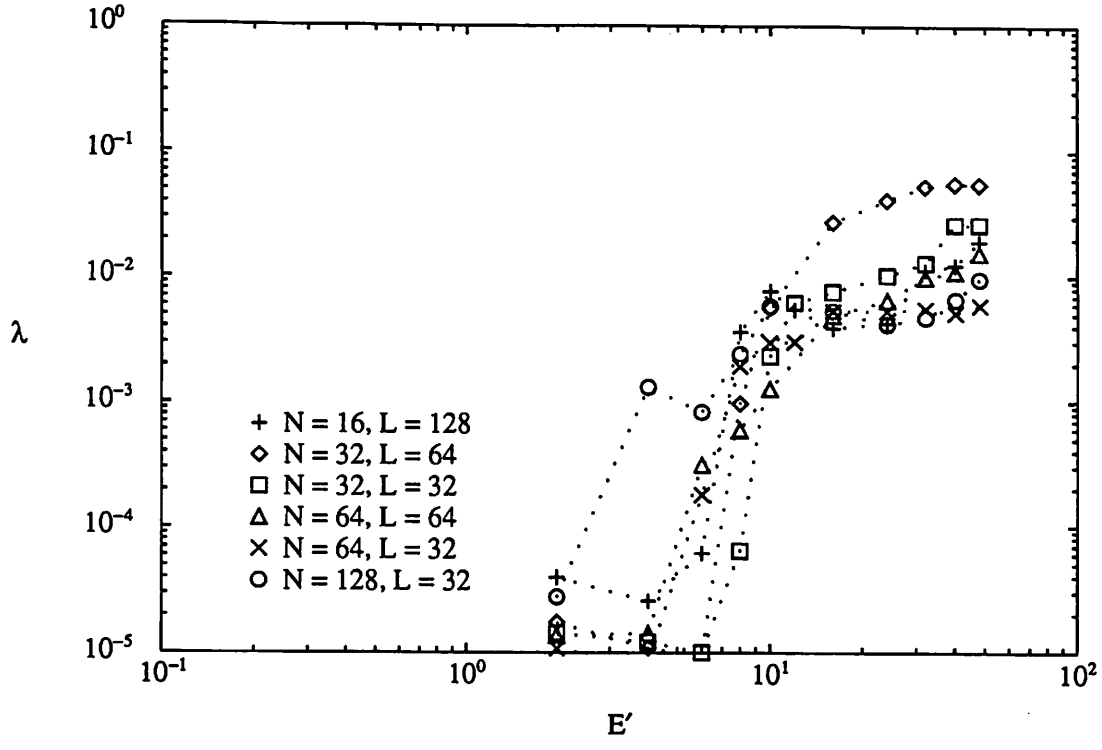
10^0
10^{-1}
10^{-2}
10^{-3}
10^{-4}
10^{-5}
λ
10^{-1}
10^0
10^1
10^2
E′
+ N = 16, L = 128
◇ N = 32, L = 64
□ N = 32, L = 32
△ N = 64, L = 64
× N = 64, L = 32
○ N = 128, L = 32

Figure 6

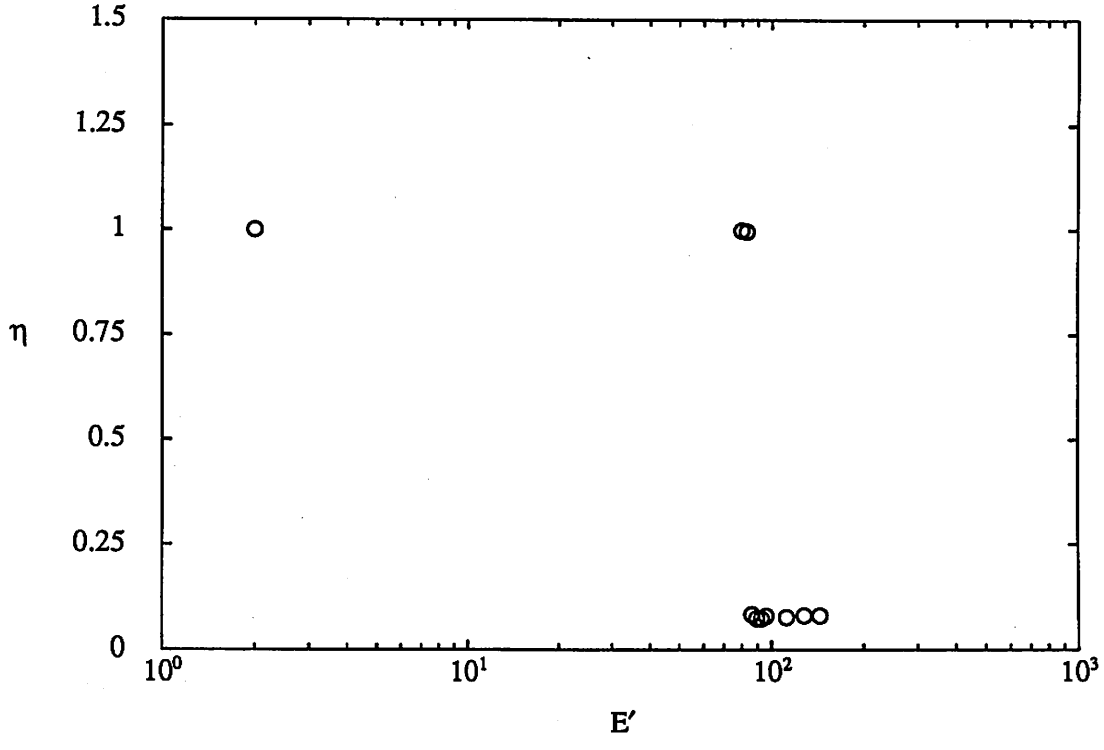

Figure 7

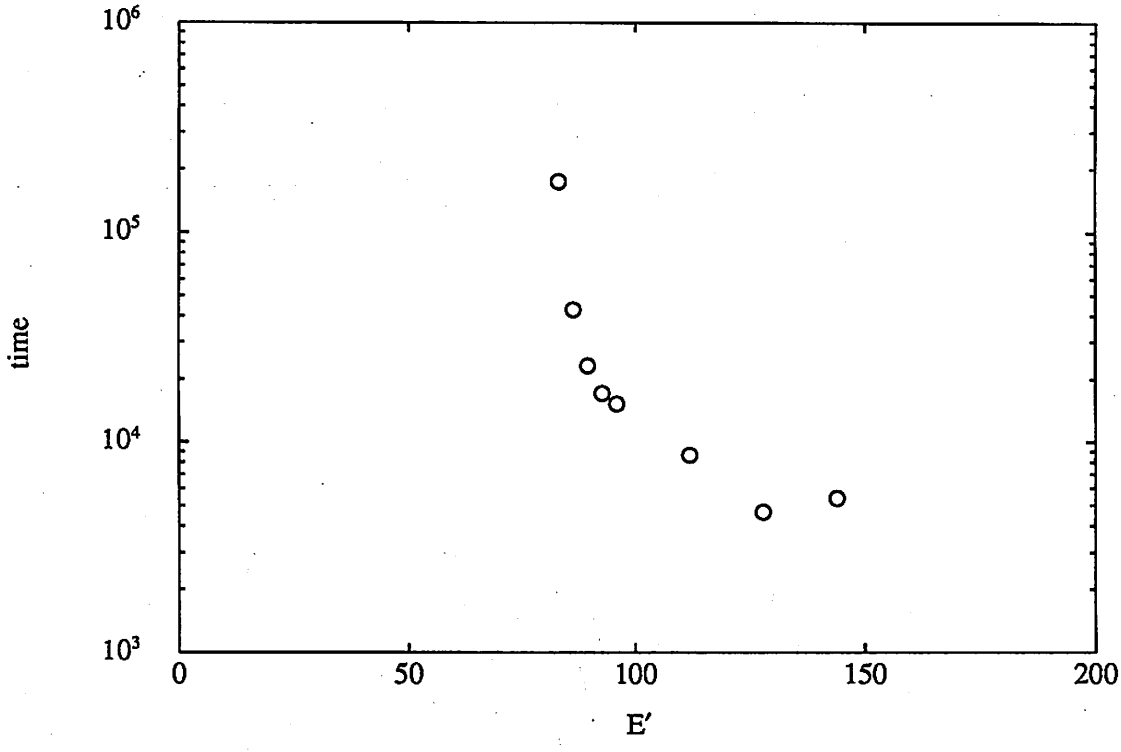

Figure 8

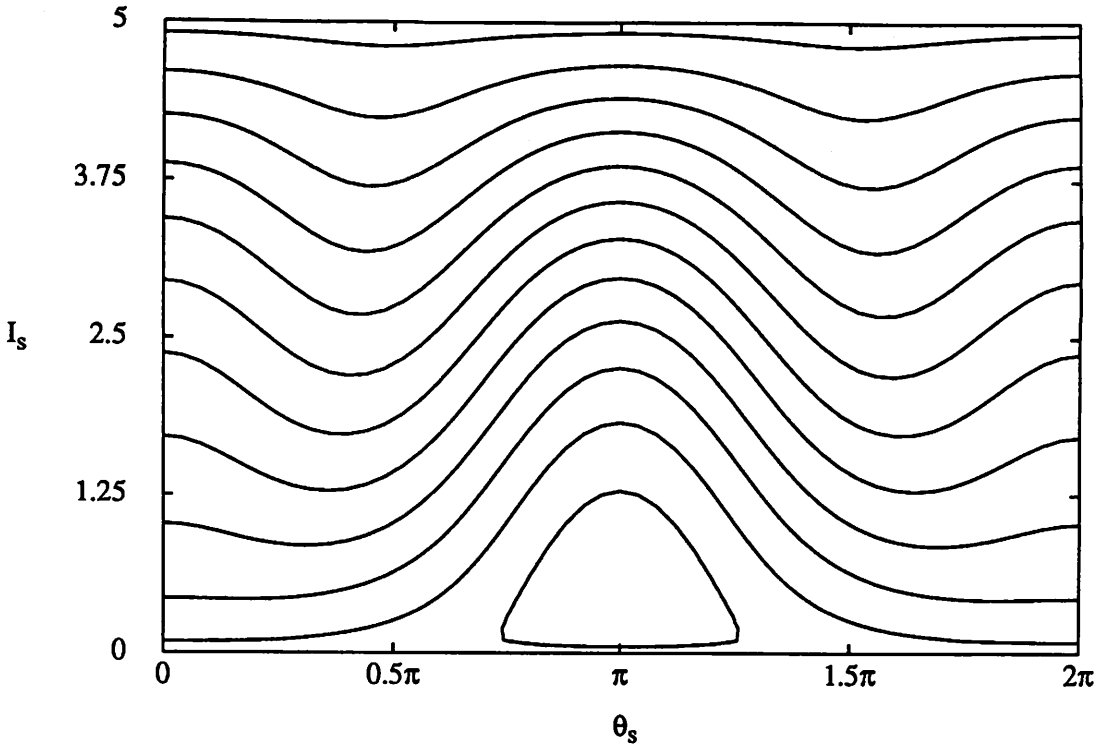

Figure 9a

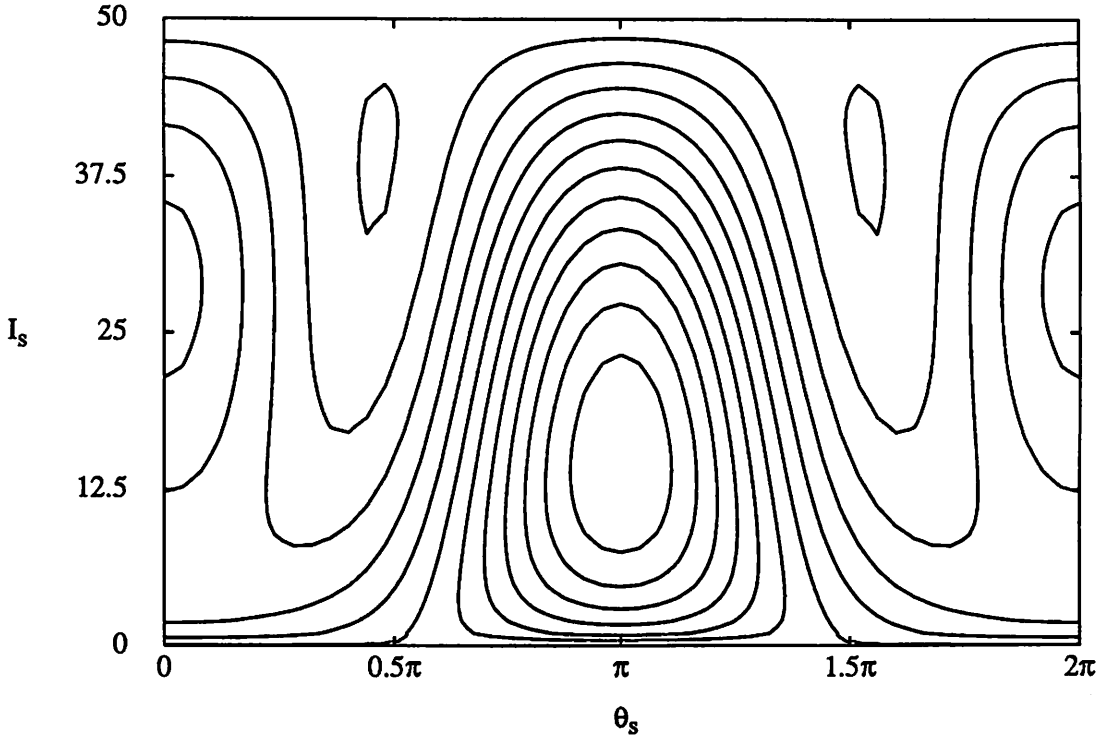

Figure 9b

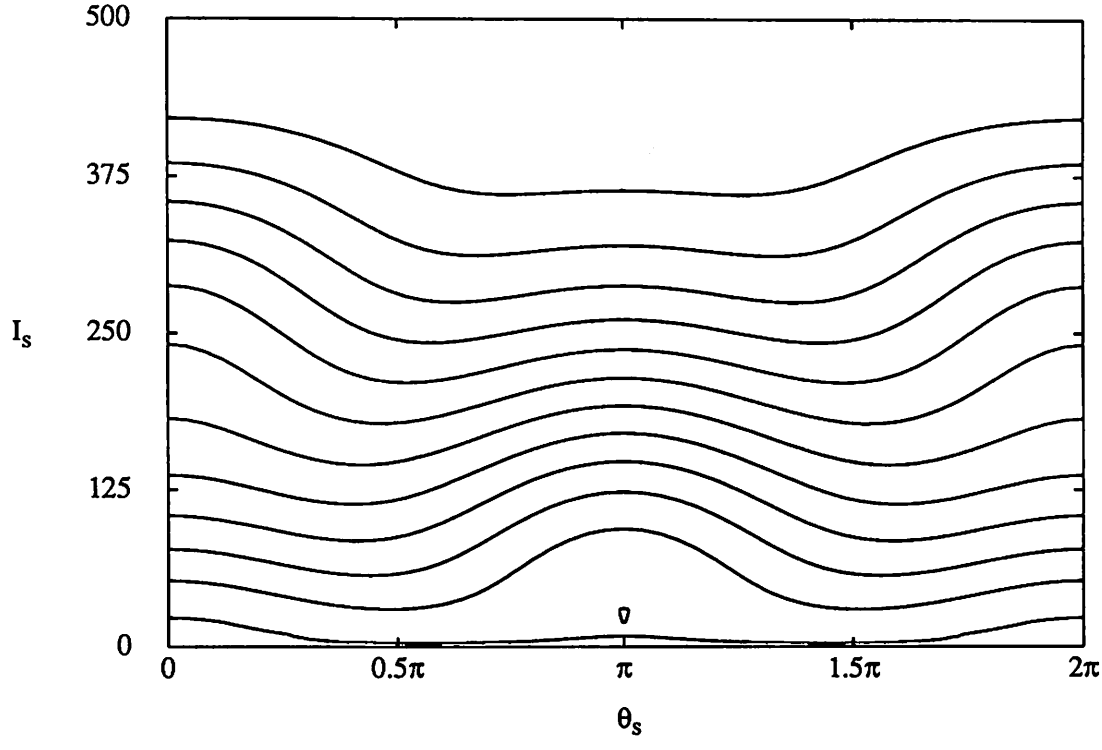

Figure 9c

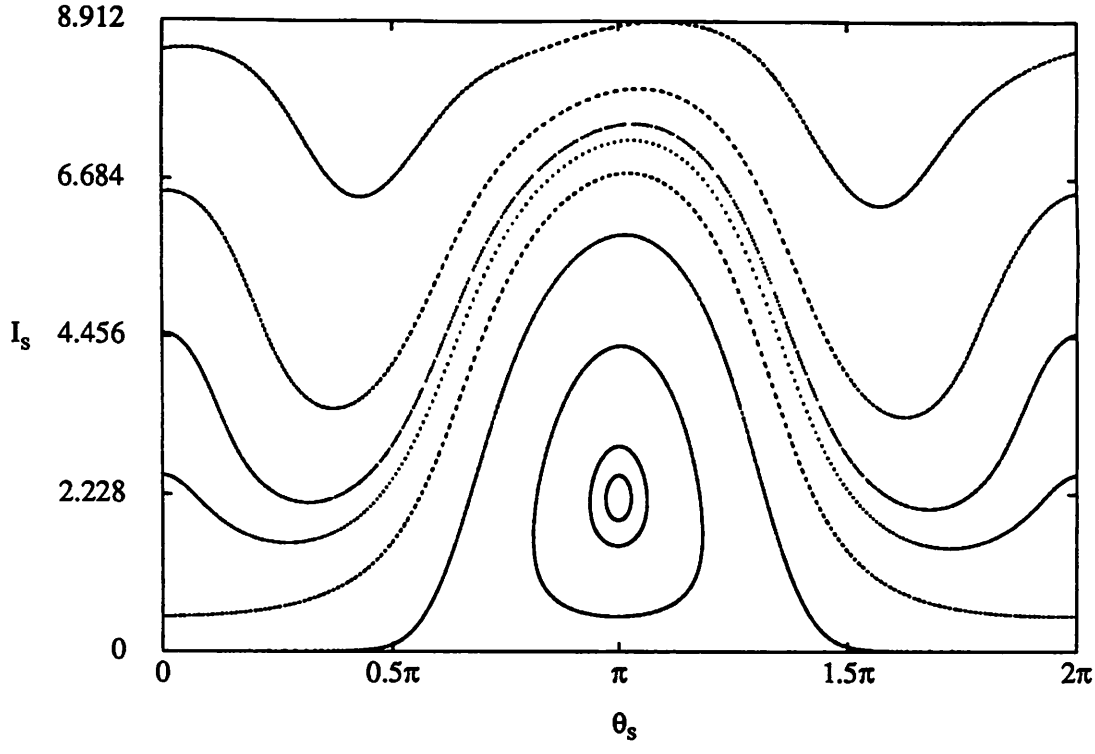

Figure 10a

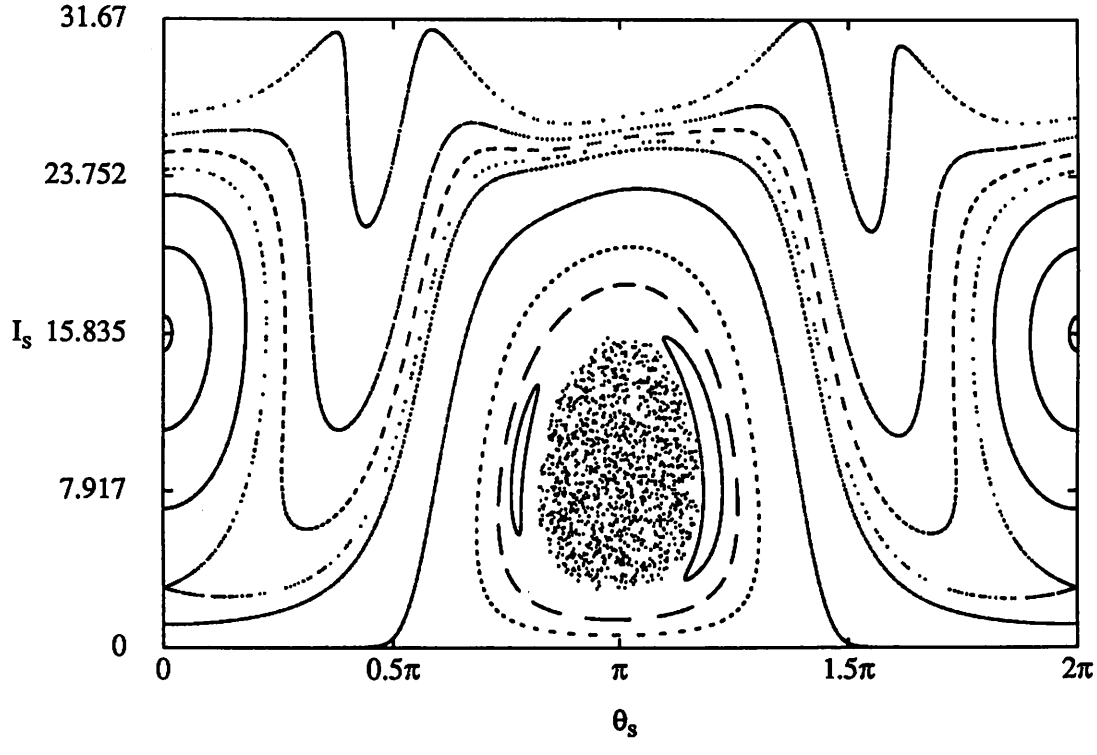

Figure 10b

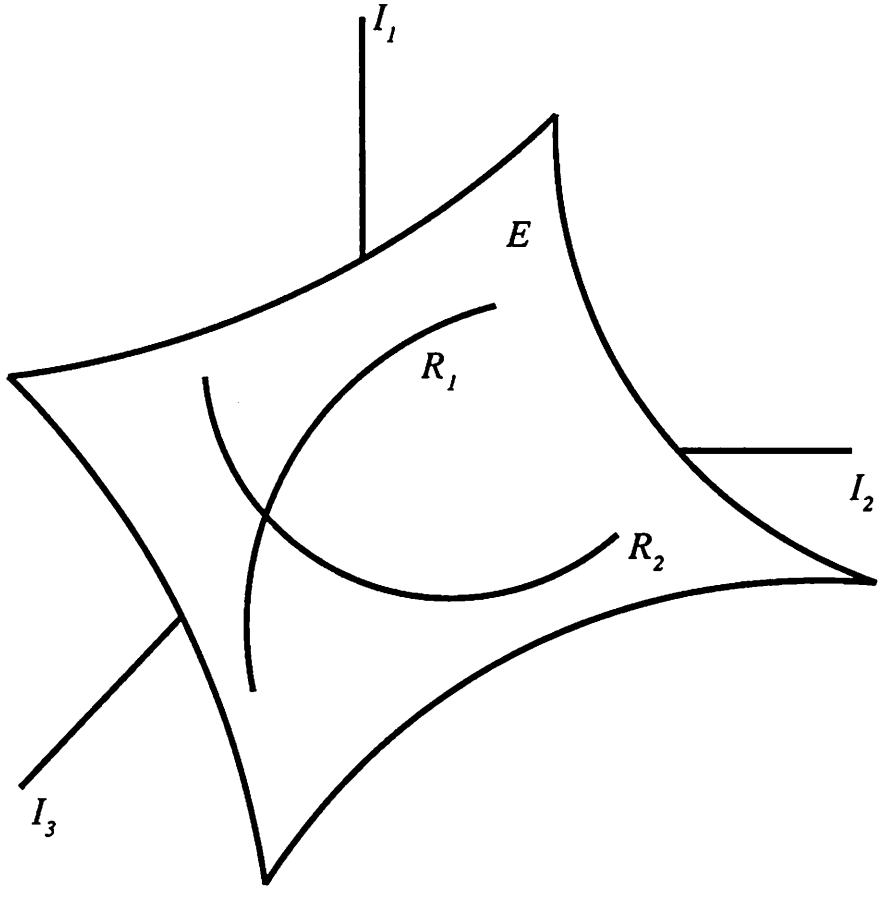

Figure 11

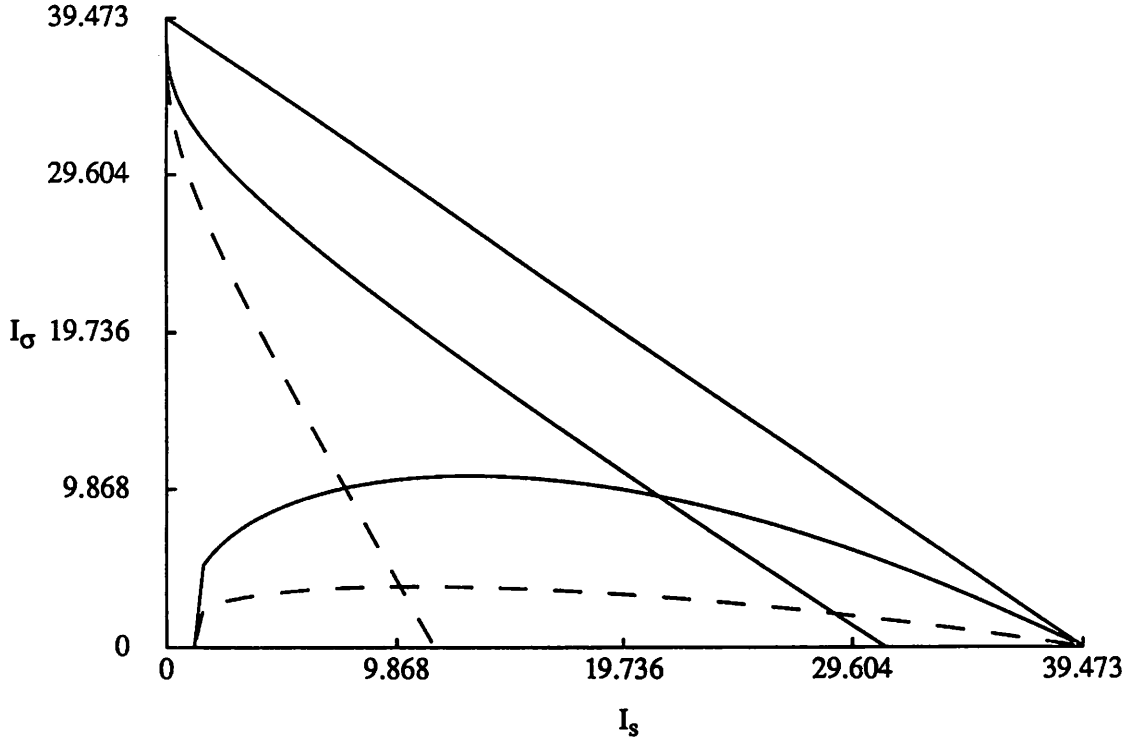

Figure 12

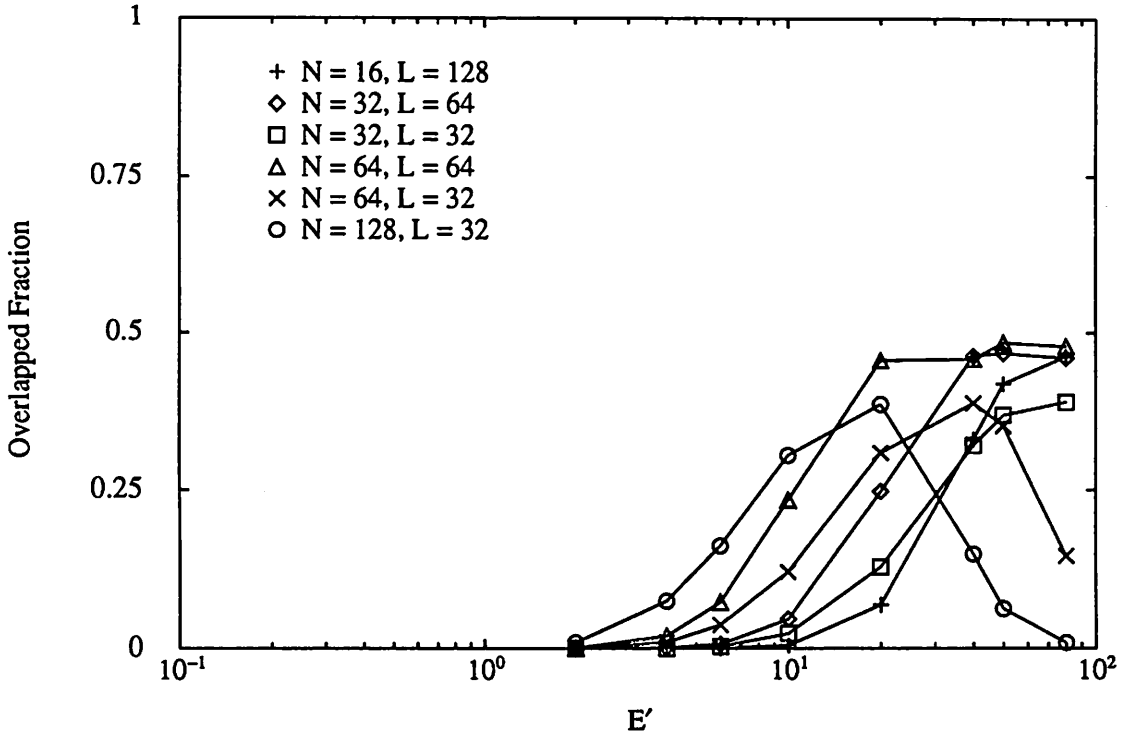
1
0.75
0.5
0.25
0
Overlapped Fraction
+ N = 16, L = 128
◇ N = 32, L = 64
□ N = 32, L = 32
△ N = 64, L = 64
× N = 64, L = 32
○ N = 128, L = 32
10^{-1}
10^{0}
10^{1}
10^{2}
E′

Figure 13

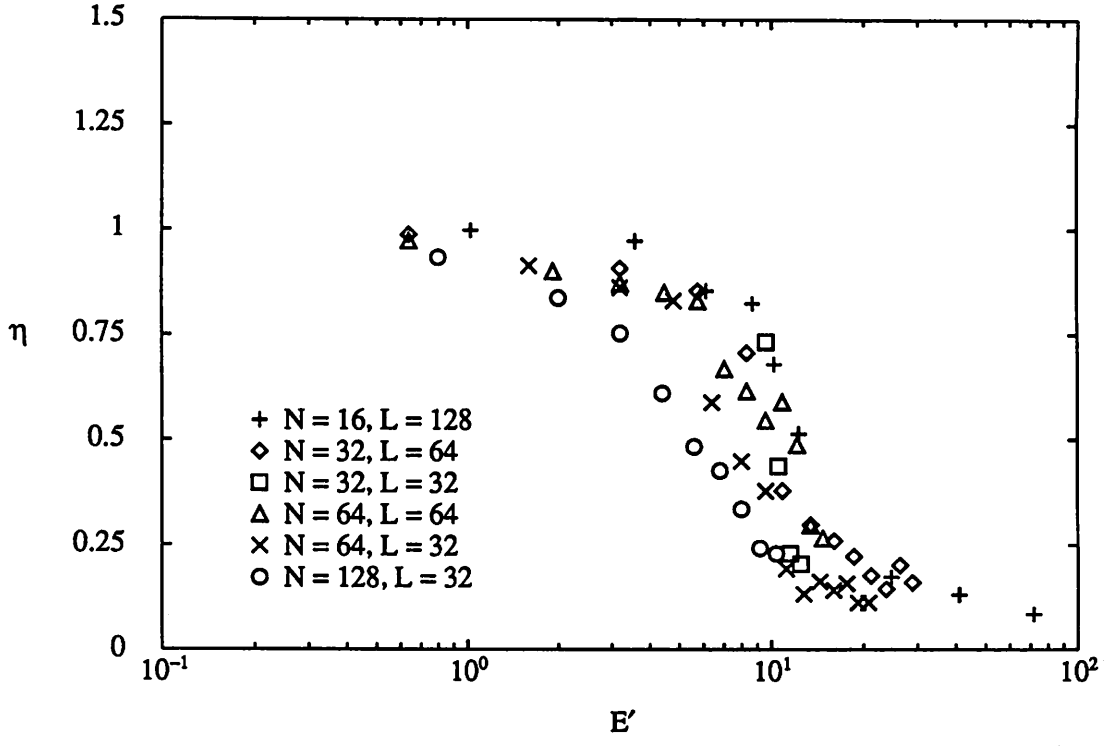
1.5
1.25
1
0.75
0.5
0.25
0
η
10^{-1}
10^{0}
10^{1}
10^{2}
E′
+ N = 16, L = 128
◇ N = 32, L = 64
□ N = 32, L = 32
△ N = 64, L = 64
× N = 64, L = 32
○ N = 128, L = 32

Figure 14